Liquid-Liquid Phase Separation of Functional Proteins and its Implication

M.Sc. Thesis

By **Rajdeep Dolai**



DEPARTMENT OF CHEMISTRY INDIAN INSTITUTE OF TECHNOLOGY INDORE

May 2025

Liquid-Liquid Phase Separation of Functional Proteins and its Implication

A THESIS

Submitted in partial fulfillment of the requirements for the award of the degree of

Master of Science

by **Rajdeep Dolai**



DEPARTMENT OF CHEMISTRY INDIAN INSTITUTE OF TECHNOLOGY INDORE

May 2025



Indian Institute of Technology Indore

CANDIDATE'S DECLARATION

I hereby certify that the work which is being presented in the thesis entitled 'Liquid-Liquid Phase Separation of Functional Proteins and its Implication' in the partial fulfillment of the requirements for the award of the degree of MASTER OF SCIENCE and submitted in the DEPARTMENT OF CHEMISTRY, Indian Institute of Technology Indore, is an authentic record of my own work carried out during the time period from August 2024 to May 2025 under the supervision of Prof. Tushar Kanti Mukherjee, Discipline of Chemistry, IIT Indore.

The matter presented in this thesis has not been submitted by me for the award of any other degree of this or any other institute.

> Rajdeep Oolai 19105/25

Signature of the student with date (RAJDEEP DOLAI)

This is to certify that the above statement made by the candidate is correct to the best of my knowledge.

Signature of the Supervisor

(Prof. Tushar Kanti Mukherjee)

Rajdeep Dolai has successfully given his M.Sc. Oral Examination held on 15th May 2025.

Signature of Supervisor of MSc thesis

Date:

ACKNOWLEDGEMENTS

Initially, I express my gratitude towards my thesis supervisor, **Prof. Tushar Kanti Mukherjee**, for providing me with valuable guidance, suggestions, and supervision, as well as for offering constant encouragement throughout my research work.

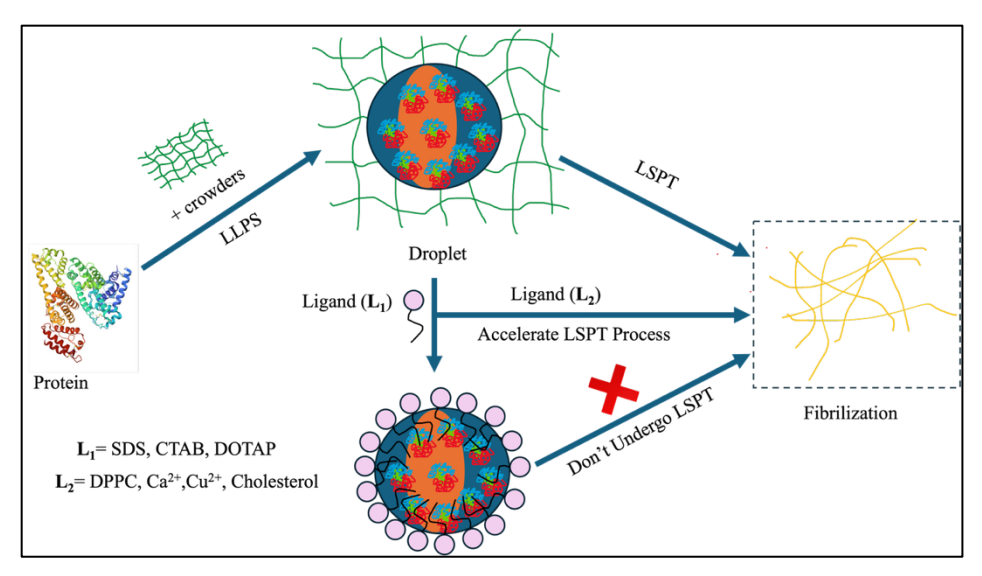
I would like to extend my gratitude to my laboratory colleagues and senior **Dr. Shivendra Singh**, **Dr. Chinmaya K. Patel**, **Mr. Supritam Datta**, **Mr. Prince Yadav**, **Mr. Saurabh Gupta and Mr. Sumit Mohapatra**, who consistently provided me with valuable insights and unwavering support in pursuit of the project's objectives. The information that you generously imparted to me was greatly motivating, not only for the present undertaking but also for the broader realm of communication practice. Further, I would like to acknowledge SIC, IIT Indore, for the instrumentation facilities and other library staff for their constant help whenever required.

I wish to express my gratitude to **Suhas S. Joshi**, Director, IIT Indore for his continuous support in every aspect.

Dedicated to My Family....

Abstract

The transition of disordered proteins from a liquid-like state to a solid-like state, often through unstable liquid-like droplets, is a wellknown biological phenomenon associated with various pathological conditions, including neurodegenerative diseases. Various ligands, including surfactants, lipids, and metal ions, affect the liquid-liquid phase separation (LLPS) and LSPT of Bovine serum albumin (BSA). Using confocal laser scanning microscopy (CLSM) assays, the results show that negatively charged surfactant sodium dodecyl sulfate (SDS), positively charged surfactant cetyltrimethylammonium bromide (CTAB) and positively charged lipid 1,2-dioleoyl-3-trimethylammonium propane (DOTAP) inhibit LSPT without affecting LLPS, preventing nucleation and fibril growth over 14 days. This effect is attributed to the electrostatic barrier formed by surfactants, reducing droplet surface tension and stabilizing phase-separated droplets. In contrast, zwitterionic DPPC, non-ionic surfactant TX-100 and metal ions like Cu²⁺ and Ca²⁺ promote early nucleation and aggregation. Secondary structure analysis through CD and FTIR revealed ligand-induced conformational changes in BSA, with reduced α -helix and increased β -sheet content. The findings suggest that ligands modulate protein-protein interactions and droplet surface properties, potentially reflecting cellular mechanisms for regulating biomolecular phase transitions and preventing protein aggregation (Scheme 1).



Scheme 1. Schematic representation shows the effect of ligand-bound BSA on the LSPT process.

TABLE OF CONTENTS

1.	List of Figures	X-XV
2.	Acronyms	xvi
3.	Chapter 1: Introduction	1
	1.1 Analysis of LCD, IDR of HSA and BSA	2-3
	1.2 LLPS of Functional Protein upon inert crowder	4-6
	1.3 LSPT of Functional Protein	6-7
	1.4 Implications of the LSPT of Globular Protein	7-8
	1.5 Effects of ligand bound on Globular Protein	9
4.	Chapter 2: Review of past work	10
	2.1 Literature Review	11-13
	2.2 Objectives	13
5.	Chapter 3: Experimental Sections	14-17
6.	Chapter 4: Results and discussions	18
	4.1 Interaction of SDS with BSA	19-21
	4.2 Interaction of CTAB with BSA	21-23
	4.3 Interaction of TX-100 with BSA	24-25
	4.4 Interaction of metal ions with BSA	25-27
	4.5 Interaction of ibuprofen and warfarin with BSA	27-29
	4.6 Interaction of DPPC with BSA	29-31
	4.7 Interaction of cholesterol with BSA	31-33
	4.8 Interaction of DOTAP with BSA	33-35
	4.9 Interaction of trypsin with SDS	36-38
7.	Chapter 5: Conclusions	39
	5.1 Conclusions	40
	5.2 Scope of future work	40-4
8.	Appendix – A	42-43
9.	References	44-48

LIST OF FIGURES

Scheme 1. Schematic representation shows the effect of ligand-bound BSA on the LSPT process.

Figure 1. (a) The Crystal structure of HSA (PDB entry 7DJN) acquired from the Protein Data Bank. (b) Analysis of the Primary Sequence of HSA Using the SMART Algorithm to Predict the LCDs and (c) IUPred2 Analysis to Predict the Disorder Tendency (UniProt Id P02768). (d) Crystal structure of BSA (PDB entry 4F5S) obtained from Protein Data Bank (e)Analysis of the Primary Sequence of BSA using the SMART Algorithm to Predict the LCDs and (f) IUPred2 Analysis to Predict the Disorder Tendency (UniProt Id P02769).

Figure 2. Separations of the homogenous phase into two liquid phases.

Figure 3. Excluded volume effect.

Figure 4. CLSM image of LLPS of BSA at day 1.

Scheme 2. Schematic representation of the pathway of LSPT.

Figure 5. Spreading of fibrils in brain various region.

Figure 6. Various neurodegenerative diseases.

Scheme 3. a) The liquid-like protein condensates formed through liquid-liquid phase separation (LLPS) are highly dynamic and constantly exchanged with the surrounding environment. With time and changes in the surrounding environment, the solidification of liquid-like condensates to hydrogels and amyloid fibrils occurs via liquid-solid phase transition (LSPT). b) Various types of multivalent interactions that promote the initiation and maintenance of LLPS include RNA-binding domains, oligomerization domains, motif-binding domains, helix-helix interactions,

β-zippers, π-π interactions, cation-anion interactions, dipole-dipole interactions, and cation-π interactions.

Scheme 4. Transition of soluble monomeric form to insoluble fiber stage.

Figure 7. Structure of SDS.

Figure 8. (a) Daylight photographs of 500 μM BSA solutions in the presence of 10% PEG and 10 mM SDS aged for day 1 and day 14. (b) CD spectra of 500 μM BSA in the absence and presence of 10% PEG and 10 mM SDS at 0 hours. (c) Confocal images of RBITC-labeled BSA droplets in the presence of 10% PEG as a function of different SDS concentrations at day 1, (d) at day 7, and (e) at day 14. The scale bars correspond to 10 μm. (f) Normalized FL intensity profile of BSA+10% PEG in the presence of different SDS concentrations.

Figure 9. (a) Deconvoluted FTIR spectra of 500 μM BSA in the absence of 10% PEG and in the presence of 10% PEG and different SDS concentrations at 0 hours. (b) The plot shows the percentage of secondary structures of BSA in the absence and presence of various SDS concentrations estimated from the deconvoluted FTIR spectra. (c) ζ potentials of BSA droplets and BSA droplets in different SDS concentrations.

Figure 10. Structure of CTAB.

Figure 11. (a) Deconvoluted FTIR spectra of 500 μM BSA in the absence and presence of 10% PEG and 2 mM CTAB at 0 hour. (b) The plot shows the percentage of secondary structures of BSA in the absence and presence of 10% PEG and 2 mM CTAB concentration estimated from the deconvoluted FTIR spectra. (c) CD spectra of 500 μM BSA in the absence and presence of 10% PEG and 2 mM CTAB at 0 hour. (d) ζ potentials of BSA droplets and BSA droplets in different CTAB concentrations. (e) Confocal images of RBITC-labeled BSA droplets in the presence of 10%

PEG as a function of different CTAB concentrations at day 1, (f) at day 7, and (g) at day 14. The scale bars correspond to 10 μm.

Figure 12. Structure of TX-100.

Figure 13. (a) Daylight photographs of 500 μM BSA solutions in the presence of 10% PEG and 0.5 mM TX-100 aged for day 1, day 7 and day 14. (b) CD spectra of 500 μM BSA in the absence and presence of 10% PEG and 0.5 mM TX-100 at 0 hours (c) Confocal images of RBITC-labeled BSA droplets in the presence of 10% PEG as a function of different TX-100 concentrations at day 1, (d) at day 7, and (e) at day 14. The scale bars correspond to 10 μm. (f) Deconvoluted FTIR spectra of 500 μM BSA in the absence and presence of 10% PEG and 0.5 mM TX-100 at 0 hour. (g) The plot shows the percentage of secondary structures of BSA in the absence and presence of 10% PEG and 0.5 mM TX-100 concentrations estimated from the deconvoluted FTIR spectra.

Figure 14. (a) Daylight photographs of 500 μM BSA solutions in the presence of 10% PEG and 0.25 mM CuCl₂ (b)10 mM CaCl₂ aged for 0 hours, day 1 and day 3. (c) CLSM images of RBITC-labeled BSA droplets in the presence of 0.25 mM CuCl₂ and (d)10 mM CaCl₂ as a function of surface ageing for 3 days. The scale bars correspond to 5 μm (e) CD spectra of 500 μM BSA in the absence and presence of 10% PEG and 0.25 mM CuCl₂ and (f)10 mM CaCl₂ at 0 hours. (g) Deconvoluted FTIR spectra of 500 μM BSA in the absence and presence of 10% PEG, 0.25 mM CuCl₂ and 10 mM CaCl₂ at 0 hours. (h) The plot shows the percentage of secondary structures of BSA in the absence and presence of 10% PEG, 0.25 mM CuCl₂, and 10 mM CaCl₂ concentrations estimated from the deconvoluted FTIR spectra.

Figure 15. (a) structure of Ibuprofen (b) Structure of Warfarin.

Figure 16. (a) Daylight photographs of 500 μ M BSA solutions in the presence of 10% PEG and 150 μ M Ibuprofen, (b) 1 mM Warfarin aged for

0 hour and day 14. (c) Deconvoluted FTIR spectra of 500 μ M BSA in the absence and presence of 10% PEG, 150 μ M Ibuprofen and 1 mM Warfarin in 0 hours. (d) CLSM images of RBITC-labeled BSA droplets in the presence of 150 μ M Ibuprofen and (e) 1 mM Warfarin as a function of surface ageing for a period of 14 days. The scale bars correspond to 10 μ m. (f) Plot showing the percentage of secondary structures of BSA in the absence and presence of 10% PEG and 150 μ M Ibuprofen and 1 mM Warfarin concentration estimated from the deconvoluted FTIR spectra. (g) CD spectra of 500 μ M BSA in the absence and presence of 10% PEG and 150 μ M Ibuprofen and (h) 1 mM Warfarin at 0 hours.

Figure 17. Structure of DPPC.

Figure 18. (a) Daylight photographs of 500 μM HSA solutions in the presence of 10% PEG and 1 mM DPPC aged 0 hour and day 1. (b) CD spectra of 500 μM HSA in the absence and presence of 10% PEG and 1 mM DPPC at 0 hours (c) Confocal images of RBITC-labeled HSA droplets in the presence of 10% PEG as a function of different DPPC concentrations at 0 hour, (d) at day 1. The scale bars correspond to 10 μm. (f) Deconvoluted FTIR spectra of 500 μM HSA in the absence and presence of 10% PEG and 1 mM DPPC at 0 hour. (g) The plot shows the percentage of secondary structures of HSA in the absence and presence of 10% PEG and 1 mM DPPC concentration estimated from the deconvoluted FTIR spectra.

Figure 19. Structure of Cholesterol.

Figure 20. (a) Daylight photographs of 500 μM BSA solutions in the presence of 10% PEG and 250 μM Cholesterol aged 0 hour and day 11. (b) CD spectra of 500 μM BSA in the absence and presence of 10% PEG and 250 μM Cholesterol at 0 hours (c) CLSM images of RBITC-labeled BSA droplet + 250 μM Cholesterol (FITC-labelled) at different time intervals. The scale bars correspond to 5 μm. (d) Deconvoluted FTIR spectra of 500 μM BSA in the absence and presence of 10% PEG and 250 μM Cholesterol

at 0 hour. (e) Plot showing the percentage of secondary structures of BSA in the absence and presence of 10% PEG 250 μ M Cholesterol concentration estimated from the deconvoluted FTIR spectra. (f) ζ potentials of BSA droplets and BSA droplets in different Cholesterol concentrations.

Figure 21. Structure of DOTAP.

Figure 22. (a) Daylight photographs of 500 μM BSA solutions in the presence of 10% PEG and 4 mM DOTAP aged 0 hour and day 14. (b) CD spectra of 500 μM BSA in the absence and presence of 10% PEG and 4 mM DOTAP at 0 hours (c) Deconvoluted FTIR spectra of 500 μM BSA in the absence and presence of 10% PEG and 4 mM DOTAP at 0 hour. (d) Plot showing the percentage of secondary structures of BSA in the absence and presence of 10% PEG 4 mM DOTAP concentration estimated from the deconvoluted FTIR spectra. (e) ζ potentials of BSA droplets and BSA droplets in different DOTAP concentrations.

Figure 23. (a) Confocal images of RBITC-labelled BSA droplets in the presence of 10% PEG as a function of different DOTAP concentrations at day 1, (b) at day 14. The scale bars correspond to $10 \mu m$.

Figure 24. (a) Deconvoluted FTIR spectra of 10 μM Trypsin in the absence and presence of 10% PEG and 10 mM SDS and 10% PEG + 10 mM SDS. (b) Plot showing the percentage of secondary structures of Trypsin in the absence and presence 10% PEG and 10 mM SDS and 10% PEG + 10 mM SDS concentration estimated from the deconvoluted FTIR spectra. (c) CD spectra of 10 μM Trypsin in the absence and presence of 10% PEG and 10 mM SDS and 10% PEG + 10 mM SDS at 0 hours (d) ζ potentials of Trypsin droplets and Trypsin droplets in present of 10 mM SDS concentrations.

Figure 25. (a) Confocal images of FITC-labelled Trypsin droplets in the presence of 10% PEG (b) + 10 mM $CaCl_2$ (c) + 10 mM $CaCl_2$ + 20 mM SDS. The scale bars correspond to 10 μ m.

Scheme 5. Schematic representation of a programmable bioreactor.

Figure 26. Various Proteins and their fibre-related diseases.

ACRONYMS

ALS Amyotrophic lateral sclerosis

AFM Atomic Force Microscopy

BSA Bovine Serum Albumin

CTAB Cetyltrimethylammonium bromide

CLSM Confocal Laser Scanning Microscopy

CSF Cerebro Spinal Fluid

DOTAP 1,2-dioleoyl-3-trimethylammonium propane

FESEM Field Emission Scanning Electron Microscopy

FTIR Fourier Transform Infrared

IDR Intrinsically Disordered Region

LCD Low complexity domain

LLPS Liquid-Liquid phase separation

LSPT Liquid-solid phase transition

PEG Polyethylene Glycol

RBITC Rhodamine B Isothiocyanate

SDS Sodium dodecyl sulfate

Chapter 1: Introduction

- 1.1 Analysis of LCD, IDR of HSA and BSA
- 1.2 LLPS of Functional Protein upon inert crowder
- 1.3 LSPT of Functional Protein
- 1.4 Implications of the LSPT of Functional Globular Protein
- 1.5 Effects of ligand bound on Functional Globular Protein

1. Introduction

The main soluble protein component of the circulatory system, serum albumins, serves various physiological purposes [1]. The ability of this class of proteins to act as transporters for many substances is their most significant characteristic. BSA has undergone some of the most in-depth research within this class of proteins, in part due to the structural similarities between BSA (isolated from cow) and human serum albumin (HSA) [2]. Both albumins have identical binding sites on subdomains IIA and IIIA and have a 76% sequence homology. The amino acids lining the binding sites are primarily hydrophobic [3]. HSA comprises a solitary polypeptide chain with a molecular weight of approximately 66 kDa and around 585 amino acids.

1.1. Analysis of LCD, IDR of HSA and BSA:

The HSA molecule is structured into three homologous domains (I, II, III), which are further subdivided into nine loops (L1-L9) through the presence of 17 disulfide linkages [4]. (Figure 1a) shows the threedimensional structure of HSA (The Crystal Structure of HSA (PDB Entry 7DJN; obtained from protein data bank). Several proteins having lowcomplexity domains (LCDs) in their amino acid sequence and intrinsically disordered regions (IDRs) have recently been found to conduct LLPS in the presence or absence of inert macromolecular crowders [5]. Simple Modular Architecture Research was employed in our study to examine the presence of LCDs and IDRs. Tool (SMART) and IUPred2 sequence prediction algorithms. SMART analysis of HSA predicted that HSA has no LCD regions (Figure 1b), and the IUPred2 algorithm revealed no disordered regions in the HSA amino acid sequence (Figure 1c). BSA has three domains (I, II, III) subdivided into nine loops (L1-L9) through disulfide linkages. (Figure 1d) shows the three-dimensional structure of BSA (The Crystal Structure of BSA (PDB Entry 4F5S; obtained from protein data bank). SMART analysis of BSA predicted that BSA has no LCD regions

(**Figure 1e**), and the IUPred2 algorithm revealed no disordered regions in the BSA amino acid sequence (**Figure 1f**). The main difference between BSA and HSA from the spectroscopic point of view is that BSA has two tryptophan residues (W¹³¹ and W²¹⁴) while HSA has only one (W²¹⁴) [6]. Several studies on BSA and HSA involving the binding of small molecules, like lipids and surfactants, based on different spectroscopic techniques have been reported earlier [7],[8],[9],[10].

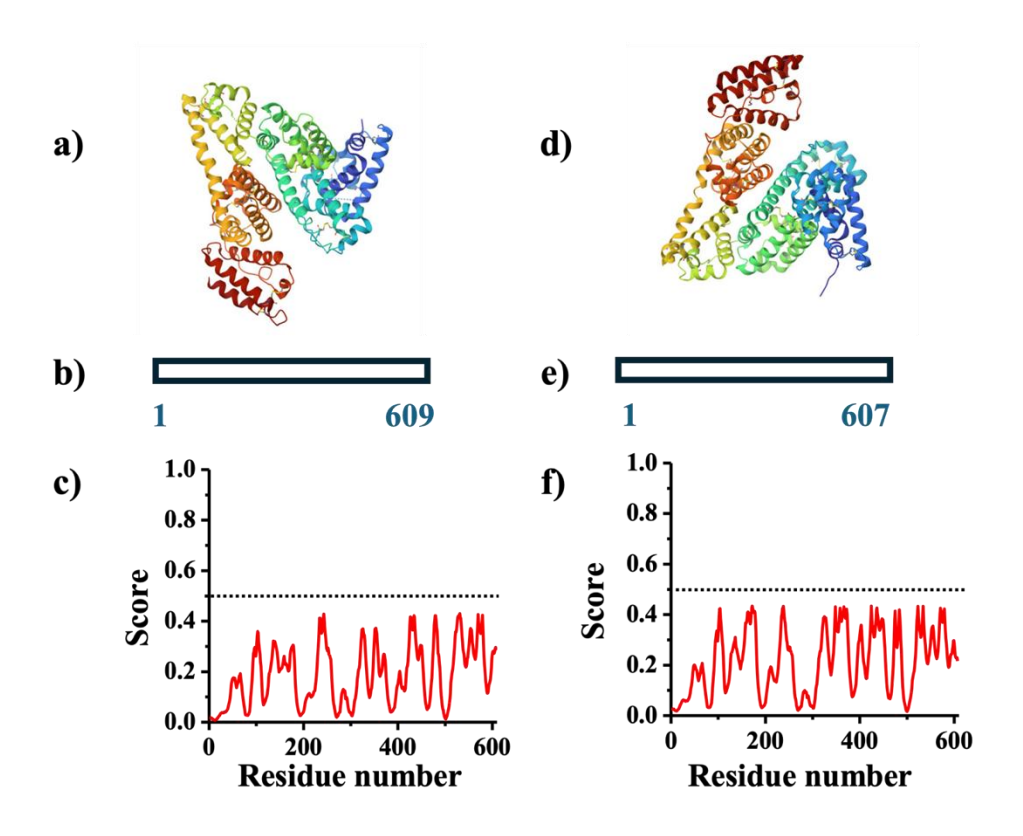


Figure 1. (a) The Crystal structure of HSA (PDB entry 7DJN) acquired from the Protein Data Bank. (b) Analysis of the Primary Sequence of HSA Using the SMART Algorithm to Predict the LCDs and (c) IUPred2 Analysis to Predict the Disorder Tendency (UniProt Id P02768). (d) Crystal structure of BSA (PDB entry 4F5S) obtained from Protein Data Bank (e)Analysis of the Primary Sequence of BSA using the SMART Algorithm to Predict the LCDs and (f) IUPred2 Analysis to Predict the Disorder Tendency (UniProt Id P02769).

1.2. LLPS of Functional Protein upon inert crowder:

Liquid-liquid phase separation (LLPS) is a process where a homogeneous mixture of two or more liquids spontaneously separates into two or more distinct liquid phases, each with different compositions and properties (**Figure 2**).

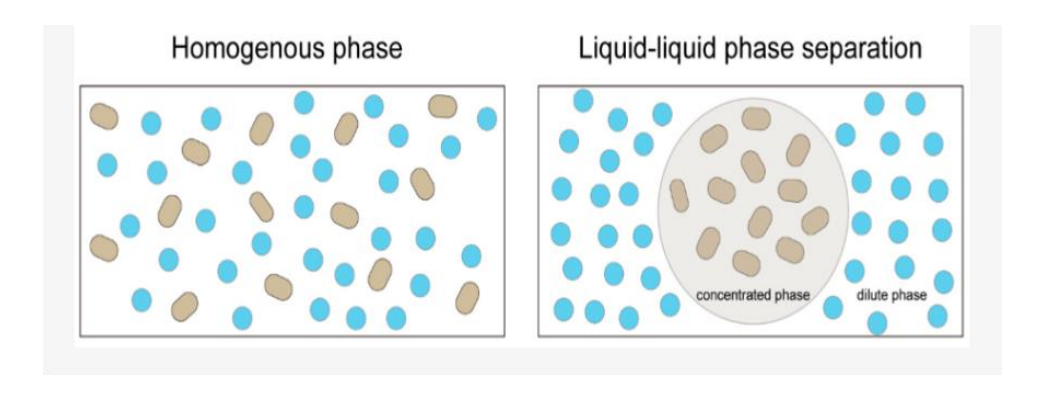


Figure 2. Separations of the homogenous phase into two liquid phases.

Membraneless organelles formed via LLPS are vital for cellular components' spatial and temporal organization. They are involved in various processes, such as chromatin reorganization, RNA metabolism, signalling, and ribosome biogenesis. LLPS is driven by IDPs/IDRs containing LCDs, resulting from thermodynamically favourable liquidliquid demixing driven by multivalent attractive interactions and entropy changes. Factors such as protein composition, concentration, temperature, pH, and ionic strength strongly influence LLPS, resulting in dynamic condensates stabilized by forces like hydrophobic, electrostatic, hydrogen bonding, and cation- π interactions. These condensates mediate cellular functions and act as intermediates in pathological protein aggregation, as seen with α -synuclein, which transitions from liquid droplets to amyloid aggregates. Interestingly, even globular proteins that do not have IDRs/LCDs can undergo LLPS under macromolecular crowding, enhancing enzymatic activities, as observed with horseradish peroxidase (HRP) and glucose oxidase (GOx) [11]. These findings highlight the dual roles of LLPS in promoting functional protein activity and facilitating aggregation

pathways, underscoring its potential in both physiological and pathological contexts.

In liquid-liquid phase separation (LLPS), molecular crowders play a crucial role in mimicking the crowded intracellular environment and inducing phase separation. These agents, like polymers, increase the effective concentration of biomolecules, forcing them to separate into distinct liquid-like phases. In our study, we took PEG 8K as crowders. In the presence of crowders, it leaves very small space for proteins, so they start to interact with each other. This phenomenon is called the excluded volume effect (**Figure 3**). This phenomenon occurs when two molecules cannot occupy the same space in a solution.

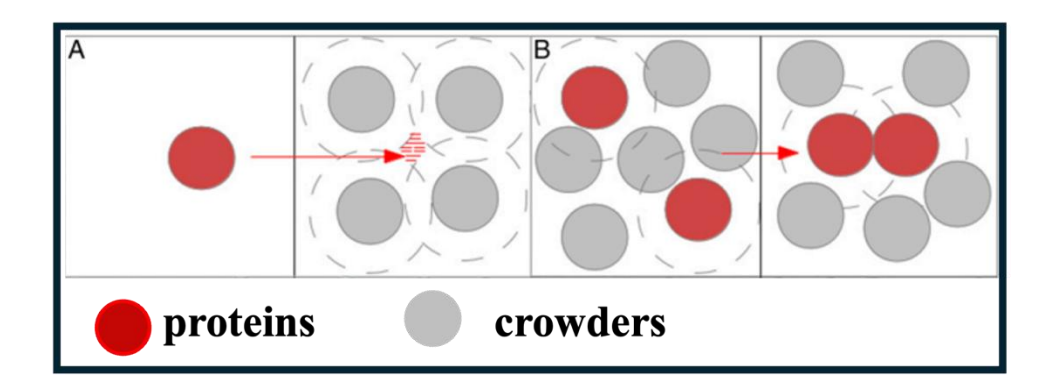


Figure 3. Excluded volume effect.

The behaviour of HSA in its distinct phase under two conditions: without any crowders, and in the presence of an inert synthetic crowder known as polyethylene glycol (PEG 8000 Da). Rhodamine B isothiocyanate (RBITC) tagged HSA at a concentration of 500 µM was used for phase behaviour investigations under a confocal laser scanning microscope (CLSM) (**Figure 4**). Day-to-day monitoring with CLSM demonstrates that droplet size grows daily, with the intermediate stage of fiber development (droplets breaking and fibers emerging from the droplets) reached at day-7 and only fibers seen by day-14. However, when PEG 8kDa is absent, HSA

exhibits no distinguishing characteristics in phase contrast or fluorescence images.

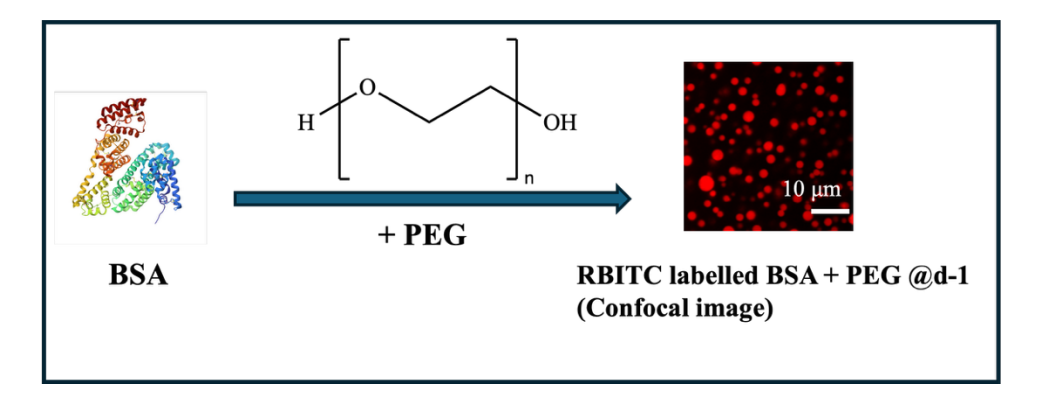
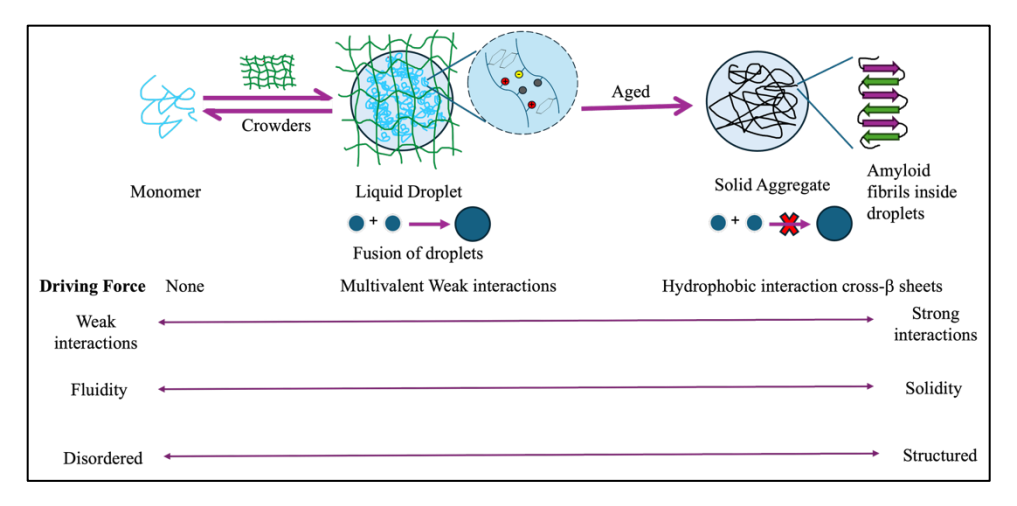


Figure 4. CLSM image of LLPS of BSA at day 1.

1.3. LSPT of Functional Protein:

Aggregation of proteins generally results from the unnatural aggregation of inherently disordered or misfolded proteins and may be divided into three structural classes: amorphous aggregates, oligomers, and amyloid fibrils. The highly structured, insoluble, and fibrillar deposition of amyloid aggregates can develop from naturally folded or intrinsically disordered proteins and become the basis for several neurodegenerative disorders. The construction of amyloid fibrils is related to several sequential associations, such as β -strands being stacked into β -sheets and interacting to create protofilaments and protofilaments stacking on or twisting around one another to form a fibril. Many factors contribute to the stability of these various protein aggregates, including hydrogen bonding between the backbone amides, van der Waals interaction between the interface of the side chains, hydrophobic interaction initiated from the hydrophobic pockets in the amino acids, electrostatic interaction, and so on (**Scheme 2**).



Scheme 2. Schematic representation of the pathway of LSPT.

1.4. Implication of the LSPT of Globular Protein:

When the liquid monomer transforms into solid fibrils this process is irreversible. It spreads from cell to cell and finally spreads over the brain's various regions and causes various neurodegenerative diseases like Alzheimer's and Parkinson's (**Figure 5**). LSPT occurs when dynamic liquid-like biomolecular condensates harden into more solid or gel-like states. This process can be beneficial by stabilizing cellular structures and regulating biological activity, but it also has pathological implications. In neurodegenerative diseases like ALS or Alzheimer's, abnormal LSPT leads to the formation of rigid, aggregated protein assemblies that disrupt cellular function. While LSPT helps organize cellular components, its dysregulation can result in toxic, irreversible deposits, making it a key factor in both normal cell regulation and disease.

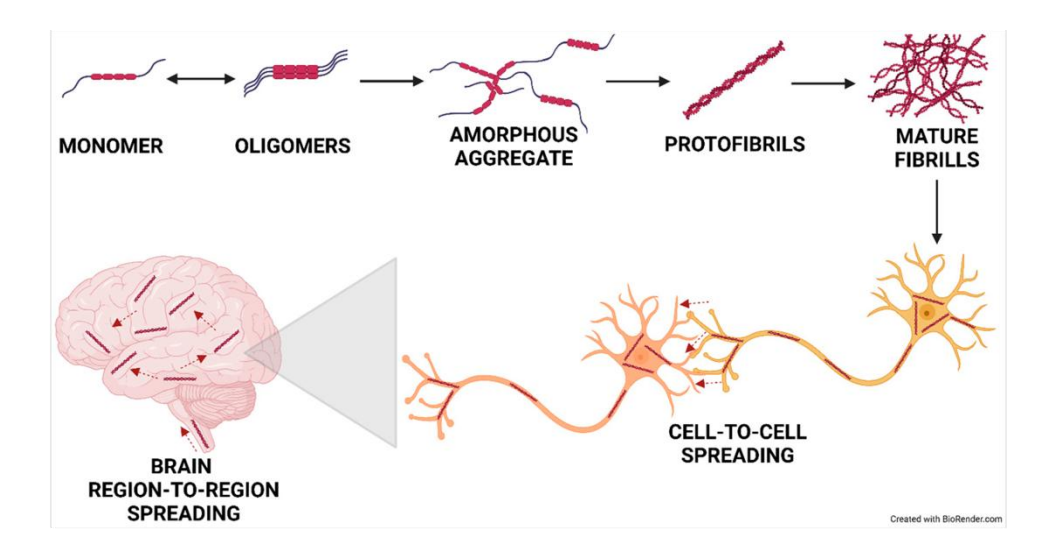


Figure 5. Spreading of fibrils in brain various region.

Various fibrils are responsible for various neurodegenerative diseases like Prp fibrils related to prion disease, A β -42 fibrils related to Alzheimer's disease, α -syn fibrils related to Parkinson's disease, IAPP fibrils related to type-2 diabetes, p53 fibrils related to cancer, phenylalanine fibrils related to inborn errors of metabolism, etc (**Figure 6**).

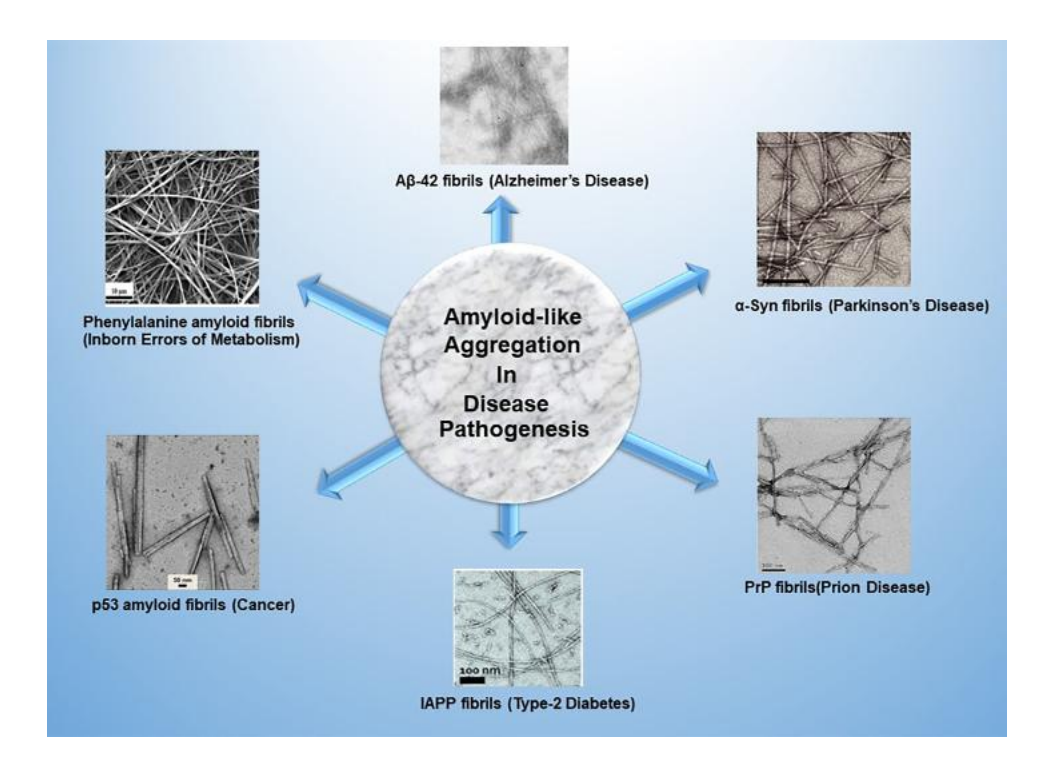


Figure 6. Various neurodegenerative diseases.

1.5. Effects of ligand bound on Globular Protein:

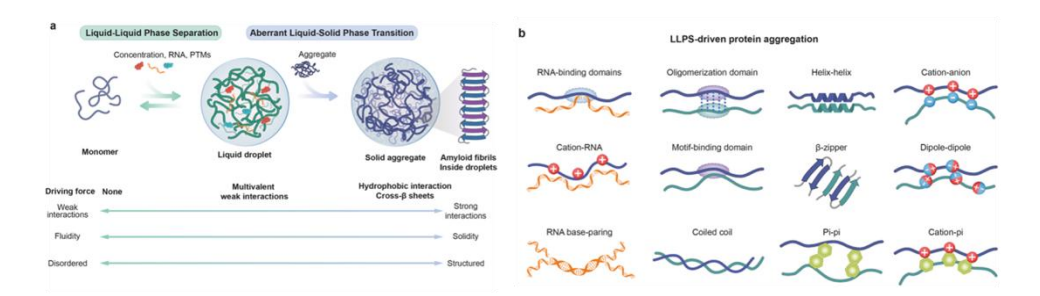
Protein-ligand binding involves a balance between entropy loss from reduced flexibility and water reorganization and enthalpy gain from favourable interactions. Van der Waals forces primarily drive binding through tight packing, while hydrogen bonds and electrostatic interactions enhance specificity but have less impact on affinity due to their presence in the unbound state. This interplay complicates predicting binding behaviours [12]. Ligand binding can significantly influence liquid-liquid phase separation (LLPS) by altering the interactions that drive condensate formation. It can modulate multivalency, either promoting LLPS by bridging protein interactions or inhibiting it by blocking interaction sites. Ligands may also induce conformational changes in proteins, such as folding or unfolding, which can respectively suppress or enhance phase separation. Additionally, ligand binding can change a protein's charge or hydrophobicity, affecting the stability and dynamics of condensates. In some cases, ligands compete with natural binding partners like RNA, thereby altering the phase behavior. These effects are crucial in both normal cellular function and in diseases where aberrant LLPS occurs.

Chapter 2: Review of Past Work

2.1 Literature review

2.2 Objectives

2.1. Literature review:



Scheme 3. a) The liquid-like protein condensates formed through liquid-liquid phase separation (LLPS) are highly dynamic and constantly exchanged with the surrounding environment. With time and changes in the surrounding environment, the solidification of liquid-like condensates to hydrogels and amyloid fibrils occurs via liquid-solid phase transition (LSPT). b) Various types of multivalent interactions that promote the initiation and maintenance of LLPS include RNA-binding domains, oligomerization domains, motif-binding domains, helix-helix interactions, β -zippers, π - π interactions, cation-anion interactions, dipole-dipole interactions, and cation- π interactions [13].

Liquid-liquid phase separation (LLPS) is a reversible and dynamic process that forms non-toxic condensed phases crucial for cellular functions. However, LLPS can progress to a liquid-solid phase transition (LSPT), where hydrophobic interactions form solid aggregates. These aggregates are typically irreversible and toxic, eventually adopting amyloid structures with ordered cross-β-sheet formations (**Scheme 3a**). LLPS has been linked to various conditions, including cancer and neurodegenerative diseases like Alzheimer's, ALS, and frontotemporal dementia, though the mechanisms underlying its transition to toxic aggregates remain primarily unclear [13]. The LSPT of functional globular proteins via metastable liquid-like droplets is poorly understood compared to disordered proteins despite its biological significance and link to pathological conditions [14].

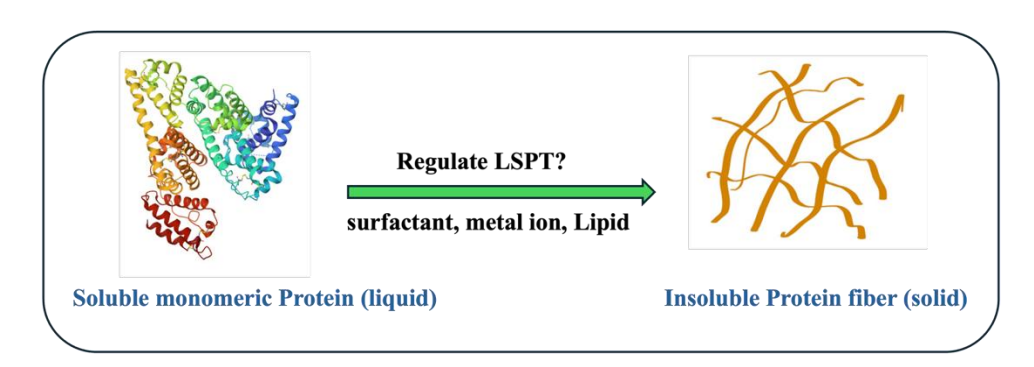
Proteins with intrinsically disordered regions (IDRs) have a simplified structure and are highly flexible and dynamic. This structural flexibility exposes them to their surroundings, increasing their chances of interacting with other intracellular molecules. Phase separation arises from the combined effects of multiple weak interactions between amino acid residues and macromolecules such as proteins and nucleic acids. Electrostatic interactions are significant in heterotypic LLPS involving protein/RNA mixtures. Other contributing forces include π - π stacking of aromatic residues, cation- π interactions (e.g., between arginine or lysine and aromatic residues like phenylalanine, tyrosine, or tryptophan), dipole-dipole interactions, hydrophobic forces, and hydrogen bonding.

Furthermore, structural motifs like oligomerization domains, coiled coils, and β-zippers create additional sites for intra and intermolecular interactions, facilitating phase separation (Scheme 3b). LSPT of human serum albumin (HSA) is driven by spontaneous droplet coalescence, facilitating nucleation and growth of amorphous aggregates that later transform into amyloid-like fibrils. Immobilized droplets fail to undergo nucleation or growth, indicating the necessity of inter-droplet communication for LSPT progression. Material exchange with the dispersed phase has minimal influence on this process, while small ligand binding modulates LSPT kinetics, suggesting a regulatory mechanism for cellular control. In a dynamic heterogeneous droplet assembly of HSA and transferrin (Tf), liquid-like and solid-like phases coexist within fused droplets, leading to mixed fibrillar assemblies. These findings provide critical insights into the role of inter-droplet interactions in LSPT and its impact on the structural integrity and function of neighbouring proteins in crowded, heterogeneous environments [15].

 α -Synuclein (α -Syn) undergoes liquid-liquid phase separation (LLPS) before aggregating into amyloid structures associated with Parkinson's disease. Low pH, mutations, and phosphomimetic substitutions

promote LLPS and aggregation. In cells, α -Syn droplets form and mature into perinuclear aggresomes, regulated by microtubules. This highlights LLPS as a critical step in α -Syn aggregation and Parkinson's pathology [16]. A pH-responsive oligopeptide repeat domain undergoes liquid-liquid phase separation (LLPS) at neutral pH, forming dynamic, liquid-like droplets. These droplets mature into solid-like aggregates at acidic pH through charge transfer and non-covalent interactions, acting as a pH sensor to regulate phase transitions and self-assembly, akin to prion-like domains [17]. Tau protein undergoes liquid-liquid phase separation (LLPS), forming droplets that transition into gel-like states and eventually aggregate into neurofibrillary tangles in Alzheimer's disease. This process, observed in phosphorylated tau and disease mutants, highlights LLPS as a shared mechanism in neurodegenerative diseases [18].

2.2. Objectives:



Scheme 4. Transition of soluble monomeric form to insoluble fiber stage.

- a. How do external parameters (surfactant, metal ion, Drugs, Lipid) affect the liquid-to-solid transition of BSA?
- b. Mechanistic insight and kinetic intermediates during liquid-to-solid phase transition in the presence of different ligands.
- c. Find the application to the catalytic activity of the droplets.

Chapter 3: Experimental Section

Materials. Human serum albumin (HSA), Bovine serum albumin (BSA), polyethylene glycol 8000 (PEG 8k), fluorescein-5-isothiocyanate (FITC), rhodamine B isothiocyanate (RBITC), Hellmanex III, TX-100, Pur-A-Lyzert dialysis kit (molecular weight cutoff 3.5 kDa), cetyltrimethylammonium bromide (CTAB) was purchased from Sigma-Aldrich. Di-sodium hydrogen phosphate heptahydrate (Na₂HPO₄.7H₂O), sodium dihydrogen phosphate monohydrate (NaH₂PO₄.H₂O), calcium chloride (CaCl₂), copper chloride (CuCl₂), sodium dodecyl sulphate (SDS), sodium chloride (NaCl), and ethanol (EtOH), N-[1-(2,3dioleoyloxy)propyl]-N,N,N-trimethylammonium methylsulfate (DOTAP) were purchased from Merck. 1,2-dipalmitoyl-sn-glycero- 3-phosphocholine (DPPC) was purchased from TCI. Cholesterol ex. Sheep wool (Lanolin) was purchased from SRL. All the above chemicals were used without undergoing any additional purification steps. Eco Testr pH1 pH meter was used to adjust the PBS buffer solution's final pH (\pm 0.1).

Characterization Techniques.

Confocal Laser Scanning Microscopy (CLSM). The confocal images were collected using an inverted confocal microscope, Olympus Fluoview (model FV1200MPE, IX-83) through an oil immersion objective (100×1.4 NA). The samples were excited using two different diode lasers of 488 nm and 559 nm using appropriate dichroic and emission filters in the optical path. In the liquid-phase experiments, ~20 μL aliquot of the sample solution was drop cast into a cleaned glass slide and then sandwiched with a Blue Star coverslip. The edges of the coverslips were sealed with a minimum amount of nail paint available commercially.

Fourier-Transform Infrared Spectroscopy (FTIR). FTIR measurements were used to determine the secondary structure of the HSA and BSA using a Bruker spectrometer (Tensor-27). $\sim 10 \mu L$ of liquid samples of 500 μM

BSA and HSA in the absence and presence of 10% PEG 8k in pH 7.4 PBS buffer were used for FTIR measurement. All the spectra were recorded in the range of (4000-400 cm⁻¹). Fourier self-deconvolution (FSD) method was used to deconvolute the spectra obtained from the experiments, corresponding to the wavenumbers (1700-1600 cm⁻¹) [14]. Finally, the Lorentzian curve fits the spectra using Origin 8.1 software. All the experiments were repeated twice, and we got similar observations.

UV-vis Spectrophotometry. UV-vis Spectrophotometry was used to determine the turbidity plot. All the absorption spectra were recorded in a quartz cuvette of 3 mL (1 cm × 1 cm) using a Varian Carry 100 Bio UV-visible spectrophotometer. All the plots were plotted in Origin 8.1 software.

Fluorescence Spectroscopy. The fluorescence spectra were recorded in a quartz cuvette of 3mL (1 cm × 1 cm) using a HORIBA Jobin Yvon, model FM-100 Fluoromax-4 Spectrofluorometer at a constant temperature of 37 °C. The slit width was kept at 2 nm. All the plots were plotted in Origin 8.1 software.

Circular Dichroism (CD) Spectroscopy. CD spectra were recorded to see the structural changes in the proteins on a JASCO J-815 CD spectropolarimeter using a quartz cell (1 mL) of 1 mm path length. The scanning range was 190-260 nm. All the scans were recorded with a slit width of 1 mm, and the speed was set at 50 nm/min. For all the CD measurements, protein solutions were diluted 500-fold to make the final working concentration of 1 μ M.

Zeta Potential. Zeta potential measurements were recorded on a Brookhaven particle size analyzer (Model 90 Plus).

Fluorescence Microscope. All data were acquired on a commercial laser scanning confocal microscope (Nikon C1 with a Ti-E motorized inverted microscope) using a Plan Apochromat VC60x WI, 1.2 NA objective lens. The data were collected as an image of 2048×2048 pixels and one frame was recorded. The pixel dwell time was adjusted to $10~\mu s$. In the standard detector tab, the Gain option Pixel Time Correction was unchecked as this automatically adjusts the photomultiplier tube (PMT) gain to compensate for fluctuations in image brightness.

Chapter 4: Results & discussion

- 4.1 Interaction of SDS with BSA
- 4.2 Interaction of CTAB with BSA
- 4.3 Interaction of TX-100 with BSA
- 4.4 Interaction of metal ions with BSA
- 4.5 Interaction of ibuprofen and warfarin with BSA
- 4.6 Interaction of DPPC with HSA
- 4.7 Interaction of cholesterol with BSA
- 4.8 Interaction of DOTAP with BSA
- 4.9 Interaction of Trypsin with SDS

4.1. Interaction of SDS with BSA:

Sodium dodecyl sulfate (SDS) is an anionic surfactant with 12 carbon atoms attached to a sulfate group. It has a critical micelle concentration (CMC) at around 7 mM at 298 K in water solvent (**Figure 7**) [19].

Figure 7. Structure of SDS

We took 500 µM BSA and five different SDS concentrations above CMC and below the CMC (0.1 mM, 1 mM, 5 mM, 7 mM and 10 mM) and 10% PEG 8k as crowders. BSA transformed into solid gel at day 14 in the presence of inert crowders, but in the presence of anionic surfactant SDS, up to day 14, there was no gel formation at 10 mM SDS concentration, but below the CMC, it transformed into fibril as usual (Figure 8a). The CD data represents the alteration of Secondary Structures of Phase-Separated BSA in the presence of SDS. The spectrum of BSA shows a negative peak at ~208 nm with a weak shoulder at ~222 nm, indicating an α -helix secondary structure (Figure 8b). Rhodamine B isothiocyanate (RBITC) tagged BSA at a concentration of 500 µM was used for phase behaviour investigations under a confocal laser scanning microscope (CLSM). Day-to-day monitoring with CLSM data demonstrates that below the CMC, SDS + BSA droplets break, and fibrils form, but above the CMC, SDS + BSA droplets retain till day 14 (Figure 8c-e). This phenomenon is attributed to the electrostatic barrier formed by SDS with micelle formation, which reduces droplet surface tension and stabilises phase-separated droplets. So, up to day 14 above the CMC, we didn't observe fibril formation. A comprehensive analysis must be conducted to investigate the structural alterations linked to the phase transitions of BSA. The fluorescence (Fl) intensity of a fluorophore is influenced by its surrounding environment, indicating that alterations in the tryptophan (Trp) fluorescence intensity may be associated with modifications in the conformation of the protein. An elevation in intensity is observed (**Figure 8f**); as the SDS concentration increased, the relative intensity of the normalized fluorescence intensity decreased, and after the formation of the micelle, the intensity became almost constant.

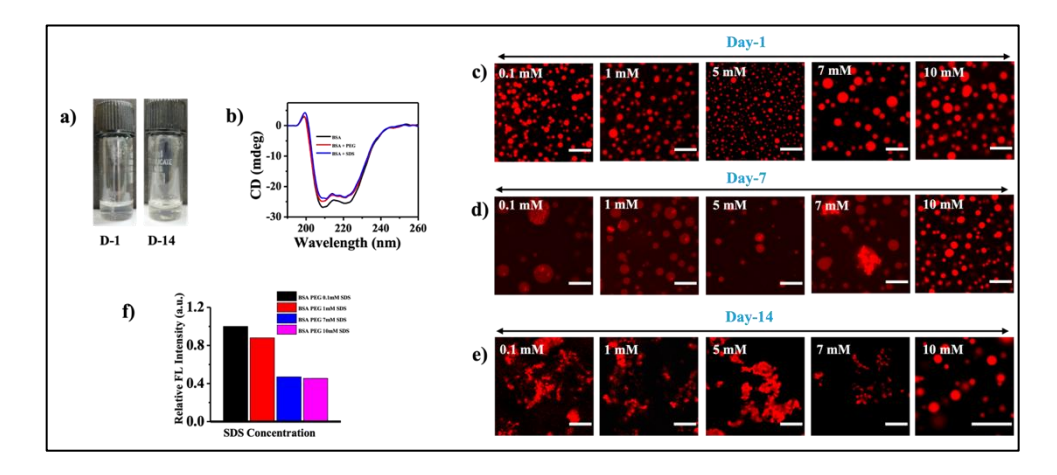


Figure 8. (a) Daylight photographs of 500 μM BSA solutions in the presence of 10% PEG and 10 mM SDS aged for day 1 and day 14. (b) CD spectra of 500 μM BSA in the absence and presence of 10% PEG and 10 mM SDS at 0 hours. (c) Confocal images of RBITC-labeled BSA droplets in the presence of 10% PEG as a function of different SDS concentrations at day 1, (d) at day 7, and (e) at day 14. The scale bars correspond to 10 μm. (f) Normalized FL intensity profile of BSA+10% PEG in the presence of different SDS concentrations.

The deconvoluted FTIR data shows the β -sheet structure was minimal in the case of only BSA, and as we add PEG, SDS different concentrations (0.1 mM, 1 mM, 10 mM), the α -helix decreased (**Figure 9a** and **Figure S1a**). The β -sheet becomes increased, which also matches the CD data. As we add PEG and different concentrations of SDS, the secondary structure becomes similar for all the other concentrations of SDS, enhancing the β -sheet structures of BSA, which is the critical factor for fast solid-like aggregation transition (**Figure 9b** and **Figure S1b**). In the

presence of SDS, droplets remained for an extended period due to the ability of SDS to maintain BSA ellipticity and prevent α -helix to β -sheet structures conversion. The Zeta potential of the BSA droplet is negative and SDS is also a negatively charged surfactant; as we mix SDS with the BSA droplet, the negative surface charge increases as the SDS concentrations increase (**Figure 9c**). This data also proves that this effect is attributed to the electrostatic barrier formed by SDS; this electrostatic charge barrier prevents droplet fusion, so fibril formation is prevented.

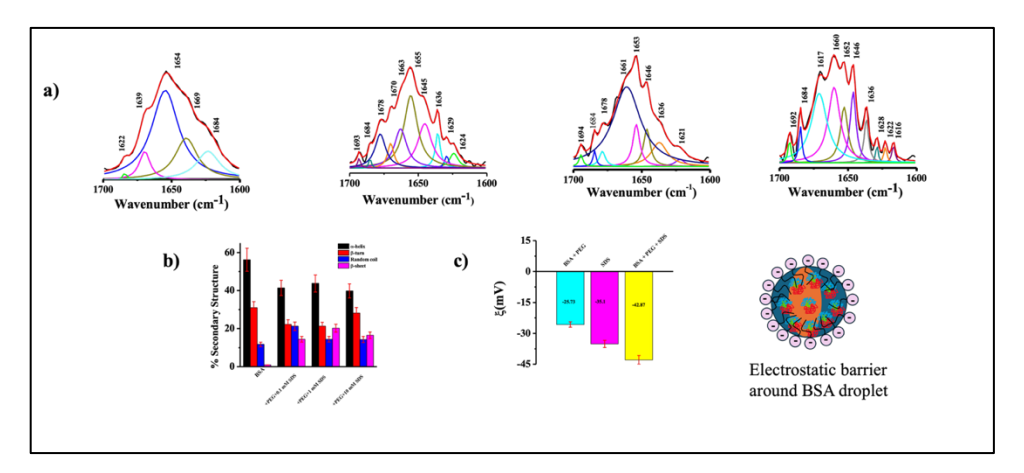


Figure 9. (a) Deconvoluted FTIR spectra of 500 μM BSA in the absence of 10% PEG and in the presence of 10% PEG and different SDS concentrations at 0 hours. (b) The plot shows the percentage of secondary structures of BSA in the absence and presence of various SDS concentrations estimated from the deconvoluted FTIR spectra. (c) ζ potentials of BSA droplets and BSA droplets in different SDS concentrations.

4.2.Interaction of CTAB with BSA:

Cetyltrimethylammonium bromide (CTAB) is a cationic surfactant with potential drug-solubilising properties and intrinsic antibacterial characteristics composed of 16 carbon tails attached to an ammonium group. It has a CMC at 0.97 mM on water solvent at 298 K (**Figure 10**) [20].

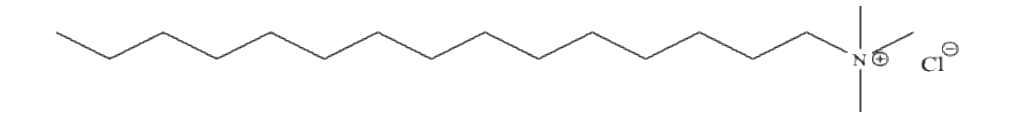


Figure 10. Structure of CTAB.

We took 500 µM BSA and five different CTAB concentrations above CMC and below the CMC (0.5 µM, 1 µM, 2 mM and 4 mM) and 10% PEG 8k as crowders. BSA transformed into solid gel at day 14 in the presence of inert crowders, but in the presence of cationic surfactant CTAB, up to day 14, there was no gel formation at 4 mM CTAB concentration, but below the CMC, it transformed into fibril as usual. The deconvoluted FTIR data shows the β -sheet structure was minimal in the case of only BSA, and as we add PEG and CTAB (2 mM), the α -helix decreased, and the β -sheet increased, which also matches with the CD data (Figure 11a). As we add PEG and 2 mM CTAB, the secondary structure becomes different for all three solutions, enhancing the β -sheet structures of BSA, which is the essential factor for fast solid-like aggregation transition (Figure 11b). In the presence of CTAB, droplets remained for an extended period due to the ability of CTAB to maintain BSA ellipticity and prevent α -helix to β -sheet structures conversion. The CD data represents the alteration of secondary structures of phase-separated BSA in the presence of CTAB. The spectrum of BSA shows a negative peak at ~208 nm with a weak shoulder at ~222 nm, indicating an α -helix secondary structure (**Figure 11c**). The Zeta potential of the BSA droplet is negative, and CTAB is a positively charged surfactant; as we mix CTAB with the BSA droplet, the droplet charge becomes positive, and as we increase the CTAB concentrations, the Zeta potentials also increase (Figure 11d). This data also proves that this effect is attributed to the electrostatic barrier formed by CTAB; this electrostatic

charge barrier prevents droplet fusion, preventing fibril formation. Rhodamine B isothiocyanate (RBITC) tagged BSA at a concentration of 500 µM was used for phase behaviour investigations under a confocal laser scanning microscope (CLSM). Day-to-day monitoring with CLSM data demonstrates that below the CMC, CTAB + BSA droplets break, and fibril formed, but above the CMC, CTAB + BSA droplets retain till day 14, and the size of the droplet becomes decreased at day 14 (**Figure 11e-g**). This phenomenon is attributed to the electrostatic barrier formed by CTAB with micelle formation, which reduces droplet surface tension and stabilises phase-separated droplets. So, up to day 14 above the CMC, we didn't observe fibril formation.

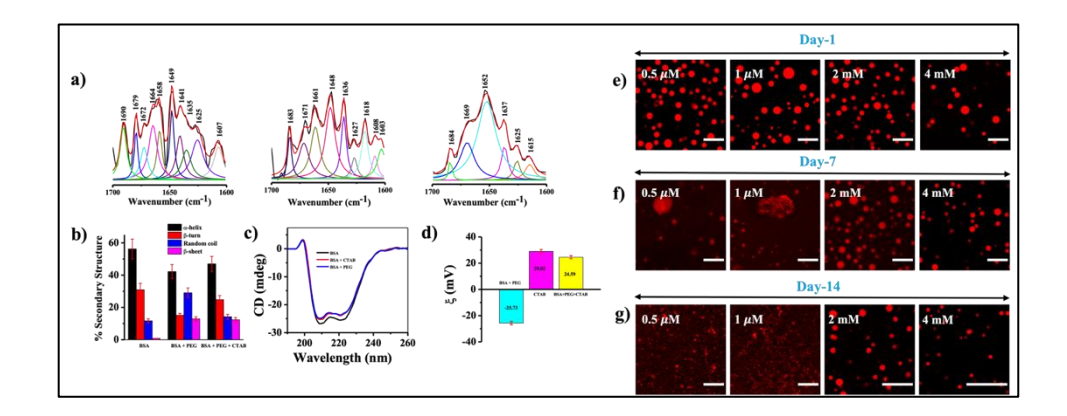


Figure 11. (a) Deconvoluted FTIR spectra of 500 μM BSA in the absence and presence of 10% PEG and 2 mM CTAB at 0 hour. (b) The plot shows the percentage of secondary structures of BSA in the absence and presence of 10% PEG and 2 mM CTAB concentration estimated from the deconvoluted FTIR spectra. (c) CD spectra of 500 μM BSA in the absence and presence of 10% PEG and 2 mM CTAB at 0 hour. (d) ζ potentials of BSA droplets and BSA droplets in different CTAB concentrations. (e) Confocal images of RBITC-labeled BSA droplets in the presence of 10% PEG as a function of different CTAB concentrations at day 1, (f) at day 7, and (g) at day 14. The scale bars correspond to 10 μm.

4.3.Interaction of TX-100 with BSA:

Triton X-100 (TX-100) is a non-ionic surfactant with a hydrophilic polyethylene oxide chain and an aromatic hydrocarbon lipophilic or hydrophobic group. It has a CMC at 0.24 mM on water solvent at 298 K (**Figure 12**) [21].

Figure 12. Structure of TX-100.

We took 500 µM BSA and three different TX-100 concentrations above CMC (0.3 mM, 0.5 mM and 1 mM) and 10% PEG 8k as crowders. Liquid BSA transformed into solid fibril at day 14 in the presence of inert crowders and, in the presence of non-ionic surfactant TX-100 (0.5 mM), above CMC BSA transformed into fibril as usual (Figure 13a). The CD data represents the alteration of secondary structures of Phase-separated BSA in the presence of TX-100. The spectrum of BSA shows a negative peak at \sim 208 nm with a weak shoulder peak at \sim 222 nm, indicating an α helix secondary structure (Figure 13b). Rhodamine B isothiocyanate (RBITC) tagged BSA at a concentration of 500 µM was used for phase behaviour investigations under a confocal laser scanning microscope (CLSM). Day-to-day monitoring with CLSM demonstrates that TX-100 + BSA droplets break above the CMC, forming fibrils (Figure 13c-e). This data conflicts with the previous experiments because TX-100 is a non-ionic surfactant, as TX-100 forms no electrostatic barrier with micelle formation, so BSA is transformed into fibril as usual. The deconvoluted FTIR data shows the β -sheet structure was minimal in the case of only BSA, and as we add PEG, TX-100 (0.5 mM), the β -sheet increases, which also matches the CD data (**Figure 13f**). As we add PEG and 0.5 mM TX-100, the secondary structure becomes different for all three solutions enhancing the β -sheet structures of BSA, which is the crucial factor for fast solid-like aggregation transition (**Figure 13g**).

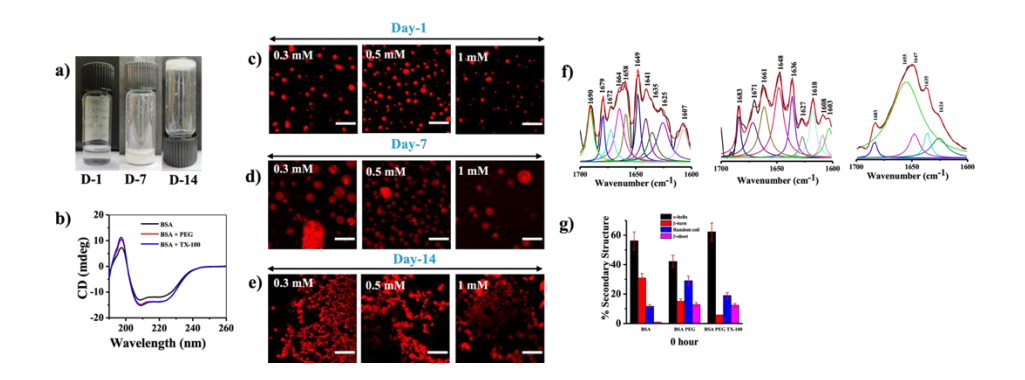


Figure 13. (a) Daylight photographs of 500 μM BSA solutions in the presence of 10% PEG and 0.5 mM TX-100 aged for day 1, day 7 and day 14. (b) CD spectra of 500 μM BSA in the absence and presence of 10% PEG and 0.5 mM TX-100 at 0 hours (c) Confocal images of RBITC-labeled BSA droplets in the presence of 10% PEG as a function of different TX-100 concentrations at day 1, (d) at day 7, and (e) at day 14. The scale bars correspond to 10 μm. (f) Deconvoluted FTIR spectra of 500 μM BSA in the absence and presence of 10% PEG and 0.5 mM TX-100 at 0 hour. (g) The plot shows the percentage of secondary structures of BSA in the absence and presence of 10% PEG and 0.5 mM TX-100 concentrations estimated from the deconvoluted FTIR spectra.

4.4.Interaction of Metal-ions with BSA:

We took 500 µM BSA and 10% PEG 8k as crowders. Liquid BSA transformed into solid fibril on day 14 in the presence of inert crowders and, in the presence of 0.25 mM CuCl₂, it catalyzes the LSPT process, and on day 3, the droplets broke and transformed into fibril (**Figure 14a**). In 10 mM CaCl₂, BSA transformed into the fibril at day 1, and LSPT became very

fast (**Figure 14b**). Rhodamine B isothiocyanate (RBITC) tagged BSA at a concentration of 500 µM was used for phase behaviour investigations under a confocal laser scanning microscope (CLSM). Day-to-day monitoring with CLSM data demonstrates that CaCl₂ catalyzes the LSPT process at day 3. For CaCl₂ day 1, the droplets break, and fibril forms significantly faster than usual (Figure 14c,d). The CD data represents the alteration of secondary structures of Phase-Separated BSA in the presence of CaCl₂ (Figure 14e). The spectrum of BSA shows a negative peak at \sim 208 nm with a weak shoulder at \sim 222 nm, indicating an α -helix secondary structure. CaCl₂ binds with BSA, the β-sheet of the Protein increases, which is confirmed with FTIR, but in the case of CuCl₂, the CD data show that the β-sheet furthermore increased, enhancing the β-sheet structures of BSA, which is the crucial factor for fast solid-like aggregation transition (Figure **14f**). The deconvoluted FTIR data shows the β -sheet structure was minimal in the case of only BSA, and as we add PEG, 0.25 mM CuCl₂ and 10 mM CaCl₂, the β -sheet increases, which also matches the CD data (**Figure 14g**). As we add PEG, 0.25 mM CuCl₂ and 10 mM CaCl₂, the secondary structure becomes different for all four solutions, enhancing the β -sheet structures of BSA, which is the crucial factor for fast solid-like aggregation transition (Figure 9h).

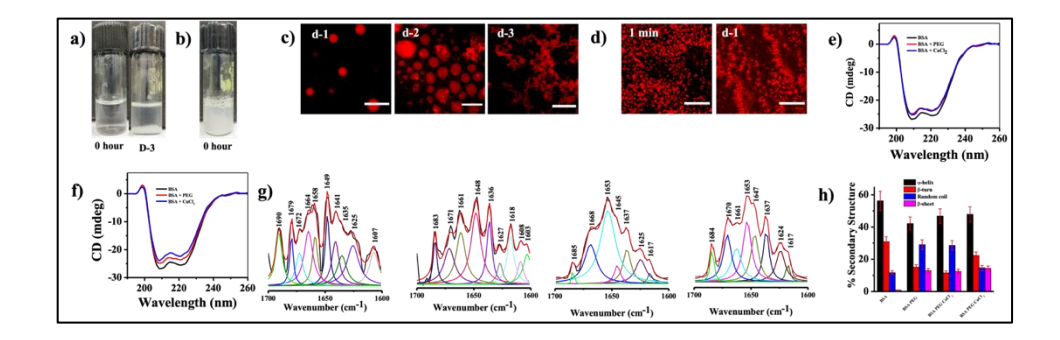


Figure 14. (a) Daylight photographs of 500 μ M BSA solutions in the presence of 10% PEG and 0.25 mM CuCl₂ (b)10 mM CaCl₂ aged for 0 hours, day 1 and day 3. (c) CLSM images of RBITC-labeled BSA droplets in the presence of 0.25 mM CuCl₂ and (d)10 mM CaCl₂ as a function of

surface ageing for 3 days. The scale bars correspond to 5 μ m (e) CD spectra of 500 μ M BSA in the absence and presence of 10% PEG and 0.25 mM CuCl₂ and (f)10 mM CaCl₂ at 0 hours. (g) Deconvoluted FTIR spectra of 500 μ M BSA in the absence and presence of 10% PEG, 0.25 mM CuCl₂ and 10 mM CaCl₂ at 0 hours. (h) The plot shows the percentage of secondary structures of BSA in the absence and presence of 10% PEG, 0.25 mM CuCl₂, and 10 mM CaCl₂ concentrations estimated from the deconvoluted FTIR spectra.

4.5.Interaction of Ibuprofen and Warfarin with BSA:

Ibuprofen is among the most commonly used drugs for pain relief, reducing inflammation, and lowering fever (**Figure 15a**). Widely available as an over the counter (OTC) medication, it is popularly surpassed only by aspirin and paracetamol for managing acute pain, inflammation, and fever symptoms [22]. Warfarin, a coumarin-based anticoagulant, is globally utilized for treating and preventing thromboembolic diseases (**Figure 15b**). However, its management is often complex due to its narrow therapeutic range and substantial interindividual variability in patient response [23].

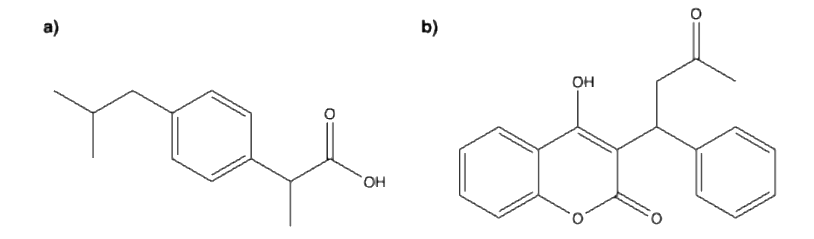


Figure 15. (a) structure of Ibuprofen (b) Structure of Warfarin.

We took 500 μ M BSA and 150 μ M Ibuprofen, 1 mM Warfarin and 10% PEG 8k as crowders. Liquid BSA transformed into solid fibril at day 14 in the presence of inert crowders and, in the presence of 150 μ M

Ibuprofen, BSA transformed into fibril faster than usual (Figure 16a). In the case of Warfarin, the BSA droplets are transformed into fibril as usual (**Figure 16b**). The deconvoluted FTIR data shows the β -sheet structure was minimal in the case of only BSA, and as we add PEG, 150 µM Ibuprofen, 1 mM Warfarin, the β -sheet increases and the α -helix increased, which also matches the CD data (**Figure 16c**). As we add PEG and 150 μM Ibuprofen, 1 mM Warfarin, the secondary structure becomes different for all four solutions, enhancing the β -sheet structures of BSA, which is the crucial factor for fast solid-like aggregation transition (Figure 16f). Rhodamine B isothiocyanate (RBITC) tagged BSA at a concentration of 500 µM was used for phase behaviour investigations under a confocal laser scanning Day-to-day monitoring with CLSM data microscope (CLSM). demonstrates that Ibuprofen catalyzes the LSPT process than usual (Figure **16d,e**). On day 14, the droplets break for Warfarin, and fibril forms as usual. The CD data represents the alteration of Secondary Structures of Phase-Separated BSA; when Ibuprofen binds with BSA, the α -helix of the Protein increases, which is confirmed with FTIR (Figure 16g). The spectrum of BSA shows a negative peak at \sim 208 nm with a weak shoulder at \sim 222 nm, indicating an α -helix secondary structure. In the case of Warfarin, similar trends were observed α -the helix of the protein increases (**Figure 16h**). So, Ibuprofen and Warfarin didn't stop the LSPT process as the BSA droplet transformed into fibril on day 14. Ibuprofen and Warfarin are non-ionic drugs, and as Ibuprofen and Warfarin form no electrostatic barrier, the BSA droplet is fused and transformed into fibril as usual.

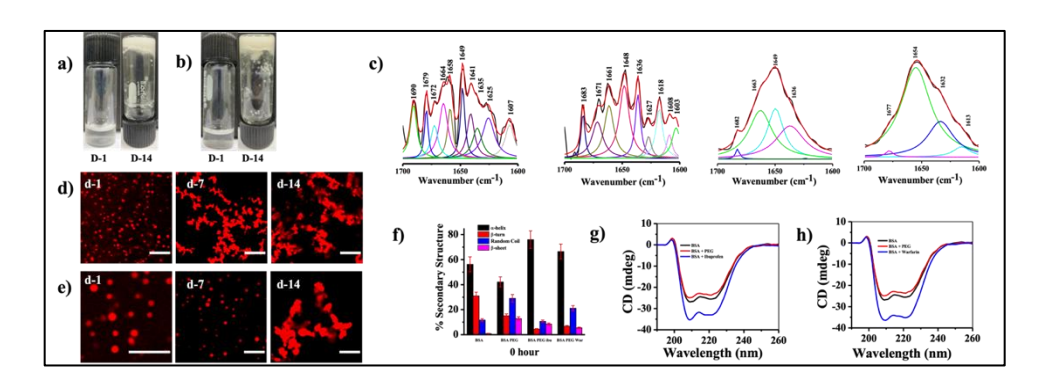


Figure 16. (a) Daylight photographs of 500 μM BSA solutions in the presence of 10% PEG and 150 μM Ibuprofen, (b) 1 mM Warfarin aged for 0 hour and day 14. (c) Deconvoluted FTIR spectra of 500 μM BSA in the absence and presence of 10% PEG, 150 μM Ibuprofen and 1 mM Warfarin in 0 hours. (d) CLSM images of RBITC-labeled BSA droplets in the presence of 150 μM Ibuprofen and (e) 1 mM Warfarin as a function of surface ageing for a period of 14 days. The scale bars correspond to 10 μm. (f) Plot showing the percentage of secondary structures of BSA in the absence and presence of 10% PEG and 150 μM Ibuprofen and 1 mM Warfarin concentration estimated from the deconvoluted FTIR spectra. (g) CD spectra of 500 μM BSA in the absence and presence of 10% PEG and 150 μM Ibuprofen and (h) 1 mM Warfarin at 0 hours.

4.6.Interaction of DPPC with HSA:

Dipalmitoylphosphatidylcholine (DPPC is a phospholipid (and lecithin) consisting of two C₁₆ palmitic acid groups attached to a phosphatidylcholine head group (**Figure 17**). It is the main constituent of pulmonary surfactants, which reduces the work of breathing and prevents alveolar collapse during breathing [24].

Figure 17. Structure of DPPC.

We took 500 μ M HSA, 500 μ M DPPC and 10% PEG 8k as crowders. Liquid HSA transformed into solid fibril at day 14 in the presence

of inert crowders, and, in the presence of 500 µM DPPC, HSA transformed into fibril much faster than usual (Figure 18a). A noticeable decrease in the α -helix and increase in the β -sheet structures of HSA is observed in the CD data representing the alteration of Secondary Structures of Phase-Separated BSA enhancing the β -sheet structures of HSA, which is the crucial factor for fast solid-like aggregation transition (Figure 18b). The spectrum of BSA shows a negative peak at ~208 nm with a weak shoulder at ~222 nm, indicating an α-helix secondary structure. same results obtained from the FTIR data. We took three different concentrations of DPPC; Rhodamine B isothiocyanate (RBITC) tagged HSA at a concentration of 500 µM was used for phase behaviour investigations under a confocal laser scanning microscope (CLSM). Day-to-day monitoring with CLSM data demonstrates that Lipid DPPC catalyzes the LSPT process, and at day 1, the droplets break, and fibril forms faster than usual (Figure 18c,d). The droplet size also noticeably increases in the case of lipid DPPC. The deconvoluted FTIR data shows the β -sheet structure was minimal in the case of only HSA, and as we add PEG, 0.5 mM DPPC, the β -sheet increases, which also matches the CD data (Figure 18e). As we add 0.5 mM DPPC, the secondary structure becomes different for all three solutions suggesting that as the β sheet increases, the structure becomes more stable. So, in the presence of Zwitter ionic lipid DPPC, we noticed early aggregation and nucleation of HSA (Figure 18f).

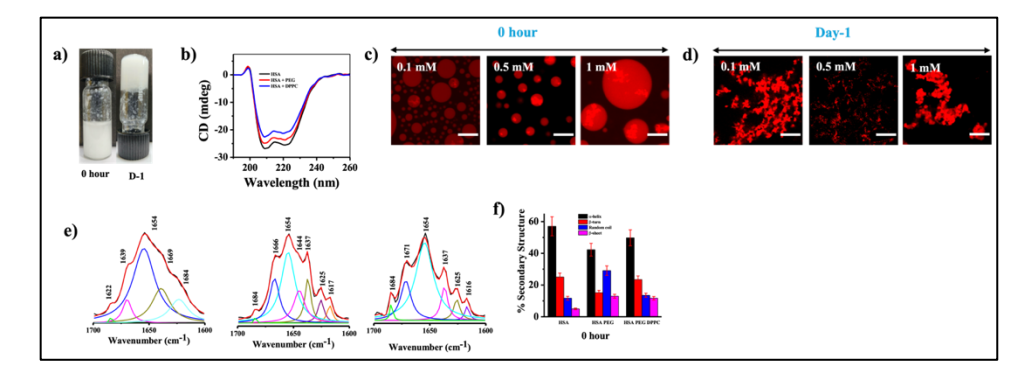


Figure 18. (a) Daylight photographs of 500 μM HSA solutions in the presence of 10% PEG and 1 mM DPPC aged 0 hour and day 1. (b) CD

spectra of 500 μ M HSA in the absence and presence of 10% PEG and 1 mM DPPC at 0 hours (c) Confocal images of RBITC-labeled HSA droplets in the presence of 10% PEG as a function of different DPPC concentrations at 0 hour, (d) at day 1. The scale bars correspond to 10 μ m. (f) Deconvoluted FTIR spectra of 500 μ M HSA in the absence and presence of 10% PEG and 1 mM DPPC at 0 hour. (g) The plot shows the percentage of secondary structures of HSA in the absence and presence of 10% PEG and 1 mM DPPC concentration estimated from the deconvoluted FTIR spectra.

4.7.Interaction of Cholesterol with BSA:

Cholesterol, a significant component of eukaryotic plasma membranes (20-40 mol%), enhances lipid order while maintaining fluidity and low permeability (**Figure 19**). Unique to cholesterol, it promotes the liquid-ordered phase, absent in membranes with lanosterol, and is crucial for forming lipid rafts and membrane domains [25].

Figure 19. Structure of Cholesterol.

We took 500 μ M BSA, 250 μ M Cholesterol and 10% PEG 8k as crowders. Liquid BSA transformed into solid fibril at day 14 in the presence of inert crowders, and, in the presence of 250 μ M Cholesterol, BSA transformed into fibril faster than usual (**Figure 20a**). A noticeable decrease in the α -helix and increase in the β -sheet structures of BSA is observed in the CD data, representing the alteration of Secondary Structures of Phase-

Separated BSA enhancing the β -sheet structures of BSA, which is the crucial factor for fast solid-like aggregation transition (Figure 20b). The spectrum of BSA shows a negative peak at ~208 nm with a weak shoulder at \sim 222 nm, indicating an α -helix secondary structure. The same results were obtained from the FTIR data. Rhodamine B isothiocyanate (RBITC) tagged BSA at a concentration of 500 µM, and Fluorescein isothiocyanate (FITC) tagged Cholesterol at a concentration of 250 µM was used for phase behaviour investigations under a confocal laser scanning microscope (CLSM). Day-to-day monitoring with CLSM demonstrates that Cholesterol catalyzes the LSPT process, and at day 11, the droplets break, and fibril forms faster than usual (Figure 20c). The droplet size also noticeably increases in the case of Cholesterol. The deconvoluted FTIR data shows the β -sheet structure was minimal in the case of only BSA, and as we add PEG, 0.25 mM Cholesterol, the β -sheet increases, which also matches the CD data (Figure 20d). As we add PEG and 0.25 mM Cholesterol, the secondary structure becomes different for all three solutions, enhancing the β -sheet structures of BSA, which is the crucial factor for fast solid-like aggregation transition (Figure 20e). The Zeta potential of the BSA droplet is negative, and Cholesterol is a negatively charged lipid, interestingly, as we mix Cholesterol with the BSA droplet, the surface charge decreases as the concentrations of Cholesterol increase (**Figure 20f**). This result differs from the previous experiments of surfactant SDS and CTAB, where, as the surfactant concentration increased, the Zeta potential increased, so Cholesterol could not prevent fibril formation.

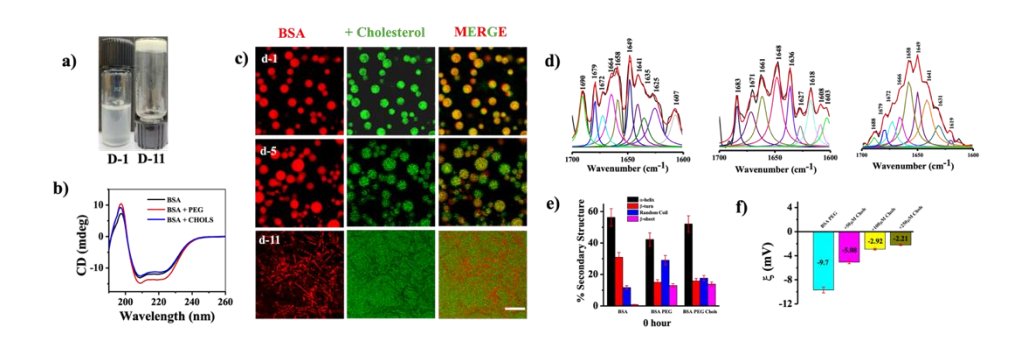


Figure 20. (a) Daylight photographs of 500 μM BSA solutions in the presence of 10% PEG and 250 μM Cholesterol aged 0 hour and day 11. (b) CD spectra of 500 μM BSA in the absence and presence of 10% PEG and 250 μM Cholesterol at 0 hours (c) CLSM images of RBITC-labeled BSA droplet + 250 μM Cholesterol (FITC-labelled) at different time intervals. The scale bars correspond to 5 μm. (d) Deconvoluted FTIR spectra of 500 μM BSA in the absence and presence of 10% PEG and 250 μM Cholesterol at 0 hour. (e) Plot showing the percentage of secondary structures of BSA in the absence and presence of 10% PEG 250 μM Cholesterol concentration estimated from the deconvoluted FTIR spectra. (f) ζ potentials of BSA droplets and BSA droplets in different Cholesterol concentrations.

4.8.Interaction of DOTAP with BSA:

Monocationic lipid DOTAP (*N*-[1-(2,3-dioleoyloxy)propyl]-*N*,*N*,*N*-trimethylammonium methylsulfate) (**Figure 21**), which is widely known as transfection lipid, consists of a monocationic trimethylammonium head group and two unsaturated hydrocarbon chains, derived of oleic acid [26].

Figure 21. Structure of DOTAP.

We took 500 μ M BSA, 5 different concentrations (0.1 mM, 0.25 mM, 0.5 mM, 2 mM and 4 mM) DOTAP, and 10% PEG 8k as crowders. Lipid is a water-insoluble substance, so we dissolve it using minimum amount of EtOH and then add PBS buffer. So, when we add DOTAP in the BSA droplets, the solution becomes turbid instantaneously. Liquid BSA

transformed into solid fibril at day 14 in the presence of inert crowders, and, in the presence of 4 mM DOTAP, up to day 14, there was no gel formation (Figure 22a). We took 1 μ M BSA concentrations for the CD study. A noticeable decrease in the α -helix and increase in the β -sheet structures of BSA is observed in the CD data, representing the alteration of Secondary Structures of Phase-Separated BSA enhancing the β -sheet structures of BSA, which is the crucial factor for solid-like aggregation transition (Figure 22b). The spectrum of BSA shows a negative peak at ~208 nm with a weak shoulder at \sim 222 nm, indicating an α -helix secondary structure. The same results were obtained from the FTIR data. The deconvoluted FTIR data shows that the β -sheet structure was minimal in the case of only BSA, and as we add PEG and DOTAP, the α -helix decreased, and the β sheet increased (Figure 22c,d). The Zeta potential of the BSA droplet is negative and DOTAP is a positively charged lipid; as we mix DOTAP with the BSA droplet, the negative surface charge gradually decreases as the DOTAP concentrations increase (Figure 22e). At high DOTAP concentrations, the surface charge becomes totally positive and increases as the DOTAP concentration increases. This data also proves that this effect is attributed to the electrostatic barrier formed by DOTAP around the BSA droplets; this electrostatic charge barrier prevents droplet fusion, so fibril formation is prevented. But at lower DOTAP concentrations, as the surface charge is low it is unable to prevent the droplets fusion as a result, the droplets transform into fibrils.

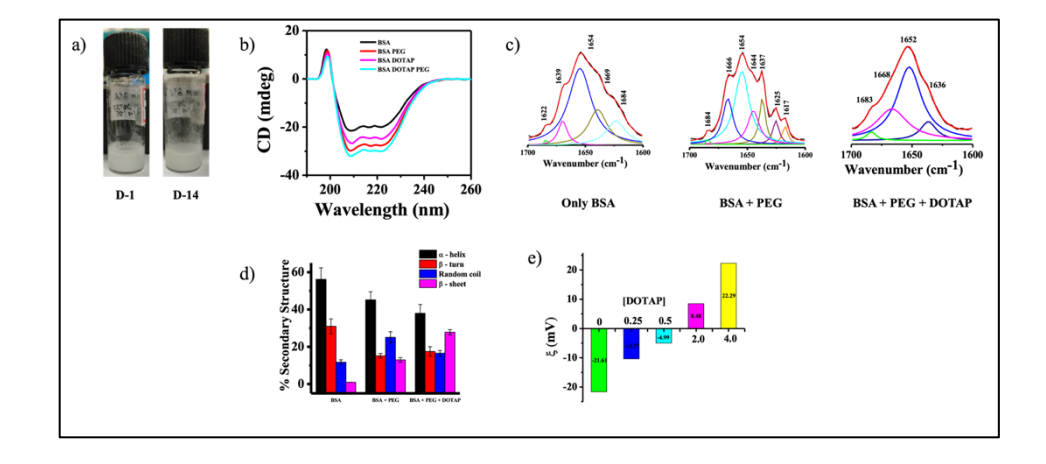


Figure 22. (a) Daylight photographs of 500 μM BSA solutions in the presence of 10% PEG and 4 mM DOTAP aged 0 hour and day 14. (b) CD spectra of 500 μM BSA in the absence and presence of 10% PEG and 4 mM DOTAP at 0 hours (c) Deconvoluted FTIR spectra of 500 μM BSA in the absence and presence of 10% PEG and 4 mM DOTAP at 0 hour. (d) Plot showing the percentage of secondary structures of BSA in the absence and presence of 10% PEG 4 mM DOTAP concentration estimated from the deconvoluted FTIR spectra. (e) ζ potentials of BSA droplets and BSA droplets in different DOTAP concentrations.

Rhodamine B isothiocyanate (RBITC) tagged BSA at a concentration of $500 \, \mu M$ was used for phase behaviour investigations under a confocal laser scanning microscope (CLSM). Day-to-day monitoring with CLSM data demonstrates that when the Zeta Potential is low, the droplets break and transform into solid fibrils, but at higher DOTAP concentrations, the Zeta potential becomes highly positive, and droplet fusion is restricted (**Figure 23a,b**).

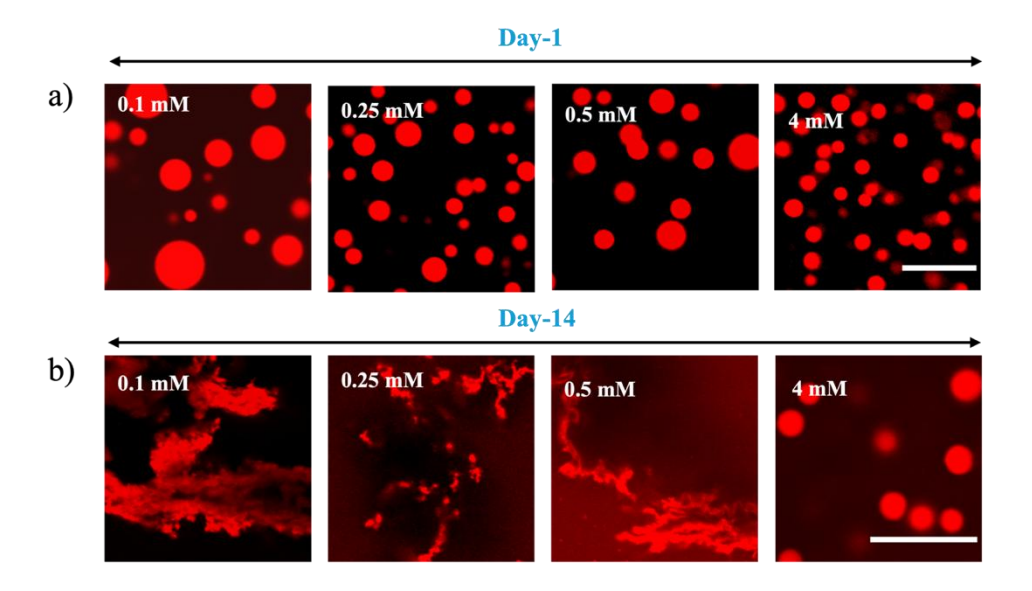


Figure 23. (a) Confocal images of RBITC-labelled BSA droplets in the presence of 10% PEG as a function of different DOTAP concentrations at day 1, (b) at day 14. The scale bars correspond to $10 \mu m$.

4.9.Interaction of SDS with Trypsin:

Trypsin is a well-characterized member of the serine protease family, with a molecular mass ranging from 23 to 25 kDa. It plays a crucial role in protein catabolism by specifically cleaving peptide bonds at the carboxyl side of basic amino acids, particularly lysine and arginine residues. Beyond its proteolytic function, trypsin also demonstrates esterase activity, facilitating the hydrolysis of ester bonds to produce corresponding carboxylic acids and alcohols. In physiological systems, trypsin is secreted into the small intestine in its active form, whereas its zymogen, trypsinogen, is synthesized in the pancreas and subsequently activated by enterokinase through site-specific proteolysis. The biosynthesis and storage of trypsin as an inactive precursor serve as a regulatory mechanism to prevent premature enzymatic activity, which could otherwise lead to pancreatic autodigestion and associated pathologies. The activity of trypsin is under stringent cellular control to prevent disorders such as pancreatitis, malabsorption syndromes, and oncogenic transformations. Structurally, trypsin-like serine proteases share a conserved catalytic triad composed of His-57, Asp-102, and Ser-195, and adopt a characteristic double β-barrel fold common to this enzyme family.

We took 10 μ M Trypsin to investigate the phase-separated behaviour of Trypsin droplets, 10 % PEG 8k as crowders for this study. To resemble the previous observation of SDS interaction with BSA droplets, we took 10 mM SDS to prevent Trypsin droplets fusion. Deconvoluted FTIR data shows that SDS bind with the trypsin droplet, as the secondary structure alternation is observed (**Figure 24a**). The β -sheet structure was maximum in the case of only Trypsin, when we add, PEG and SDS to the Trypsin droplet the β -sheet become decreased, and α -helix increased (**Figure 24b**). We took 1 mM Trypsin concentrations for the CD study. A noticeable increase in the α -helix and decrease in the β -sheet structures of Trypsin is observed in the CD data representing the alteration of Secondary Structures

of Phase-Separated Trypsin enhancing the α -helix structures of Trypsin, which is the crucial factor for solid-like aggregation transition (**Figure 24c**). The spectrum of Trypsin shows a negative peak at \sim 208 nm with a weak shoulder at \sim 222 nm, indicating an β -sheet secondary structure. The same results were obtained from the FTIR data. The Zeta potential of the Trypsin droplet is negative and SDS is a negatively charged Surfactant; as we mix SDS with the Trypsin droplet, the negative surface charge gradually increases as the SDS concentrations increase. SDS is unable to prevent Trypsin droplet fusion (**Figure 24d**).

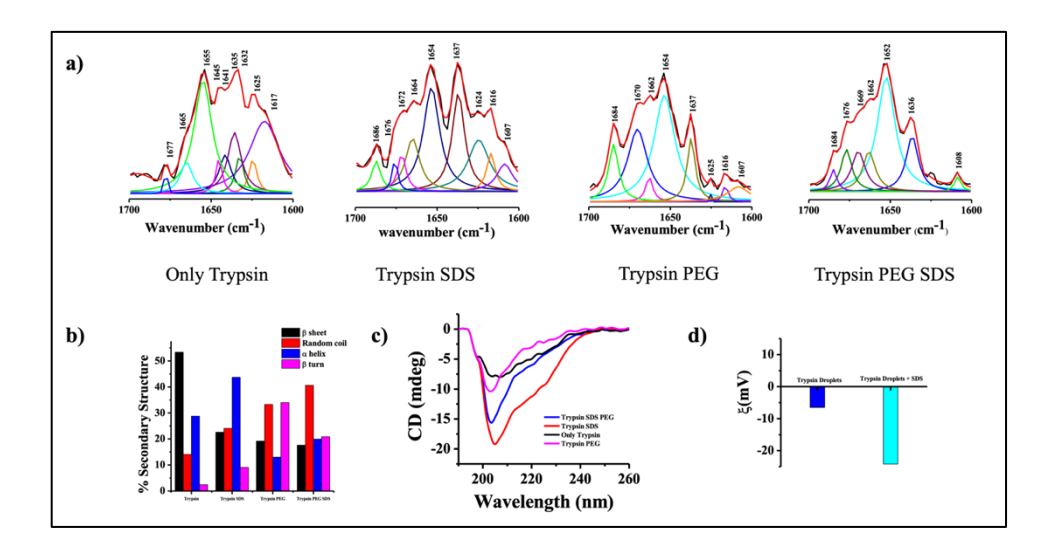


Figure 24. (a) Deconvoluted FTIR spectra of 10 μM Trypsin in the absence and presence of 10% PEG and 10 mM SDS and 10% PEG + 10 mM SDS. (b) Plot showing the percentage of secondary structures of Trypsin in the absence and presence 10% PEG and 10 mM SDS and 10% PEG + 10 mM SDS concentration estimated from the deconvoluted FTIR spectra. (c) CD spectra of 10 μM Trypsin in the absence and presence of 10% PEG and 10 mM SDS and 10% PEG + 10 mM SDS at 0 hours (d) ζ potentials of Trypsin droplets and Trypsin droplets in present of 10 mM SDS concentrations.

Fluorescein isothiocyanate (FITC) tagged Trypsin at a concentration of $10 \mu M$ was used for phase behaviour investigations under a confocal laser scanning microscope (CLSM). CLSM data demonstrates that crowders

drive the phase separation of biomolecules and stabilize the phase-separated condensates (**Figure 25a**).

Our group previously reported that the addition of 10 mM Ca^{2+} into the phase-separated trypsin results in the complete disappearance of droplets, suggesting spontaneous binding of Ca^{2+} with the phase-separated trypsin (**Figure 25b**). Firstly, we add 10 mM SDS to the Trypsin droplets, then we add 10 mM Ca^{2+} to the solution and incubate at $37 \,^{\circ}$ c. SDS is unable to prevent Trypsin droplets fusion, so Ca^{2+} binds with the phase-separated trypsin, and once again the droplets disappear (**Figure 25c**).

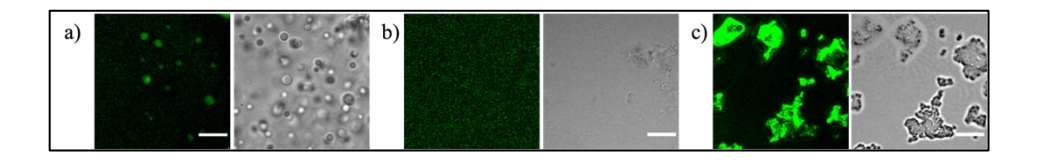


Figure 25. (a) Confocal images of FITC-labelled Trypsin droplets in the presence of 10% PEG (b) + 10 mM $CaCl_2$ (c) + 10 mM $CaCl_2$ + 20 mM SDS. The scale bars correspond to 10 μ m.

Chapter 5: Conclusions

- 5.1 Conclusions
- 5.2 Scope of future work

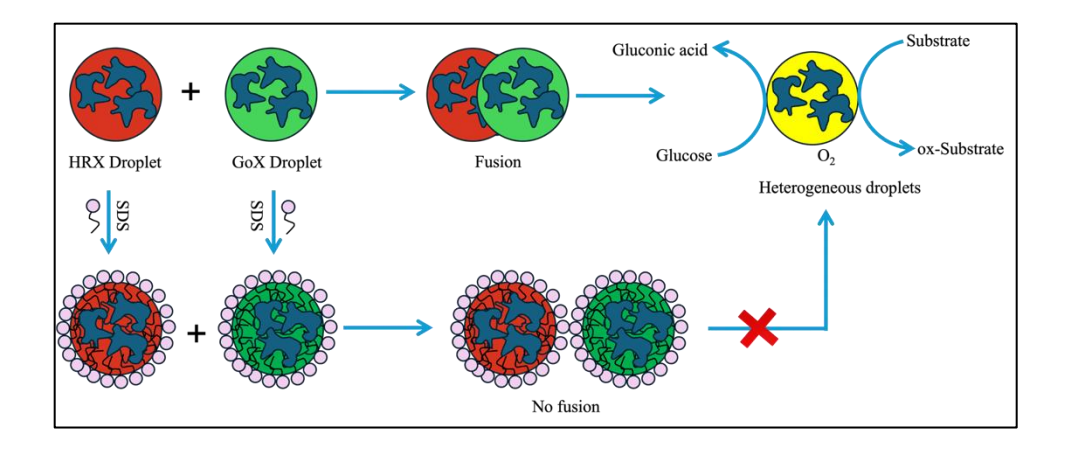
5.1 Conclusions:

In conclusion, the study highlights how various ligands, including surfactants and metal ions, significantly influence the liquid-to-solid phase transition (LSPT) of bovine serum albumin (BSA) within phase-separated droplets. Negatively charged SDS and positively charged CTAB, DOTAP inhibit LSPT by forming electrostatic barriers, reducing surface tension, and stabilizing droplets, thereby preventing nucleation and fibril growth. In contrast, zwitterionic DPPC, non-ionic TX-100, Cholesterol and metal ions like Cu²⁺ and Ca²⁺ promote early nucleation and aggregation by altering protein conformations. These findings emphasize the role of ligands in modulating protein-protein interactions and droplet surface properties, shedding light on potential mechanisms for regulating biomolecular phase transitions and preventing pathological protein aggregation in biological systems. On the other hand, SDS fails to prevent the loss of structural integrity and LSPT of trypsin, likely due to the inherent instability of the enzyme and the binding of SDS to its active site, which disrupts enzymatic function.

5.2 Scope of future work:

a) Make programmable bioreactor:

Enzyme GoX and HRP both make droplets in the presence of Crowders. HRP droplets and Gox droplets fused with each other and made heterogeneous droplets. In the presence of O₂, these heterogeneous droplets reduce glucose to gluconic acid and oxidised substrate. If we bind this HRP droplet and GoX droplet with surfactant (SDS or CTAB) they will be unable to fuse with each other. As a result, in the presence of glucose and O₂, the solution mixture will be unable to oxidise the substrate (**scheme 5**). Thus, we can make a programmable bioreactor.



Scheme 5. Schematic representation of a programmable bioreactor.

b) Using different proteins to study LLPS:

Expanding this work to other proteins and biologically relevant conditions may aid in developing strategies for controlling protein aggregation in drug design and disease treatment (**Figure 26**).

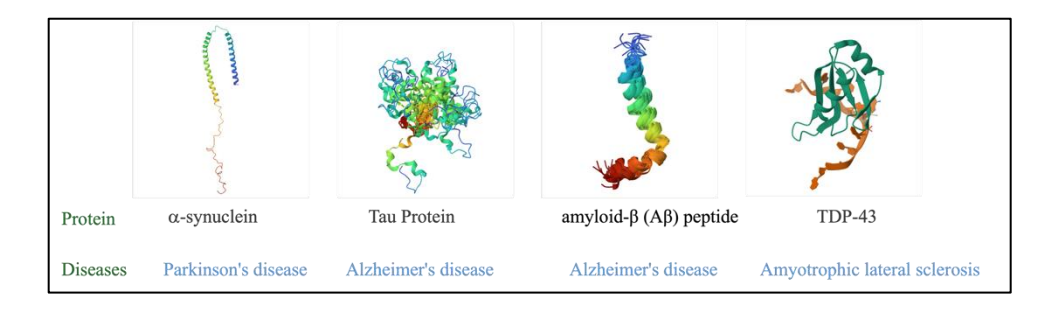


Figure 26. Various Proteins and their fibre-related diseases.

APPENDIX - A

Supporting Data:

1. Methods

- **1.1. Prediction of LCDs and IDRs of BSA and HSA:** To predict the presence of low complexity domains (LCDs) and disorder regions (IDRs) in the amino acids sequence of BSA, HSA we used Simple Molecular Architecture Research Tool (SMART) and IUPred2, respectively. 1,2 The IUPed2 data were plotted using the origin 8.1 software.
- **1.2. Preparation of Buffer Solutions and Crowder Solutions**: All the buffer solutions were prepared in the presence of 0.02% sodium azide and sterilized by autoclaving to minimise the growth of bacteria. Buffer solutions with a pH value of 7.4 were prepared using Milli-Q water. The buffer strength was kept constant at 50 mM. The crowder solution, such as 10% (w/v) PEG 8000, was prepared from a stock solution of 40% (w/v) PEG 8000. 20 mg/mL BSA was prepared from the stock solution of 332 mg/mL BSA. 20 mg/mL HSA was prepared from the stock solution of 332 mg/mL HSA.
- **1.3.** Labelling of Protein and Cholesterol with Fluorescent: BSA and HSA were labelled with RBITC dye according to an earlier reported method. In short, 1 μM BSA was mixed with RBITC in a molar ratio of 1:10 ([BSA]: [RBITC]). The mixture was incubated for 4 h at room temperature followed by 6 h, at 4 °C on a magnetic stirrer with constant speed (250 rpm). After the completion of the reaction, the unconjugated dyes were removed using dialysis (molecular weight cut-off 3.5 kDa) against 50 mM pH 7.4 phosphate buffer at 4 °C for 12 h with regular buffer exchange in 2 h intervals. The same procedure was followed for labelling Cholesterol with FITC and HSA with RBITC.

1.4. Sample Preparation

Liquid Phase Aging: Bare BSA, HSA and BSA, and HSA droplet solutions were kept at 37 °C inside an incubation chamber for the required days of ageing. For CLSM, 20 μL aliquot was withdrawn from the solutions, dropcast over a cleaned glass slide, and then immediately covered with a cleaned coverslip. The coverslips and glass slides were cleaned with 2% Hellmanex III and chromic acid. Each of these cleaning steps was followed by repeated washing with Milli-Q water. Finally, these washed slides and coverslips were rinsed with methanol and dried in a vacuum oven.

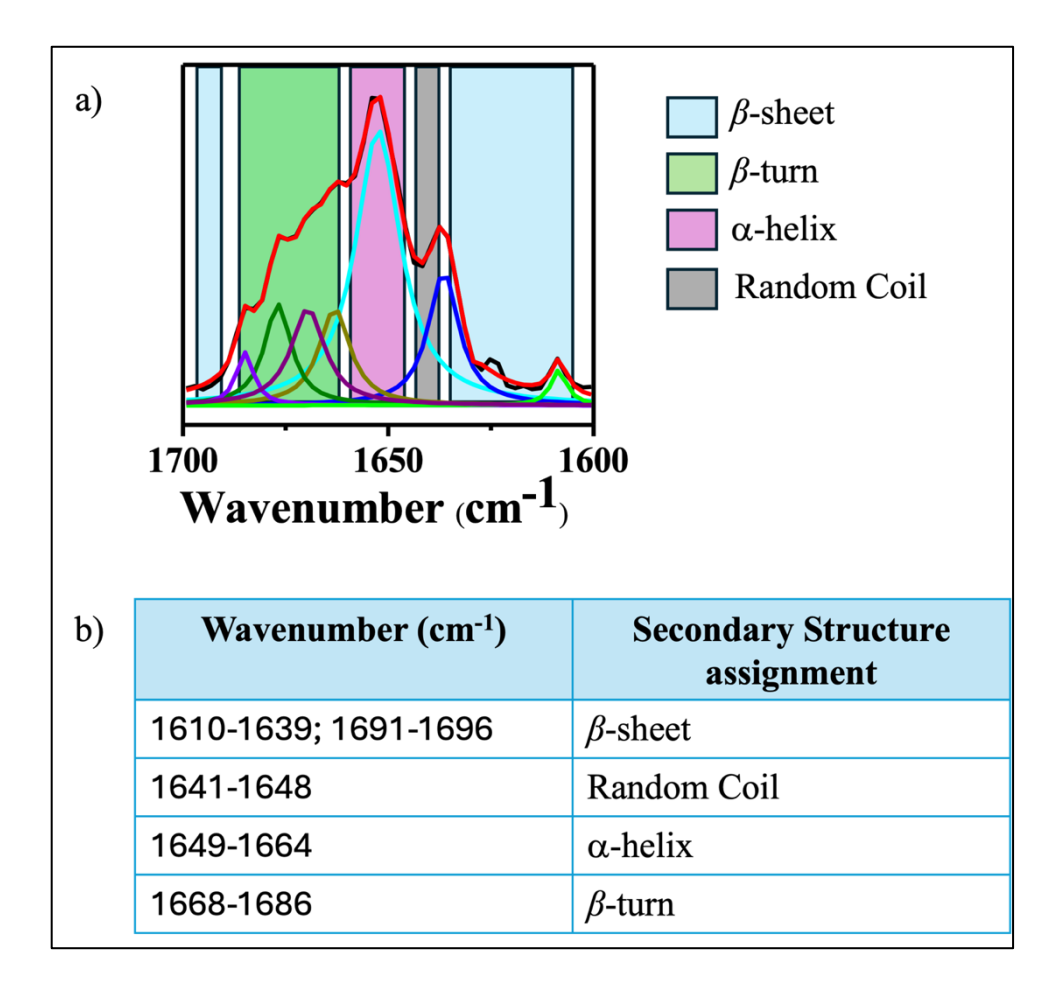


Figure S1. (a) Deconvoluted FTIR spectrum and (b) associated secondary structures of BSA in the amide I band region. Secondary structure contents were estimated by calculating the relative area under each peak using Origin 8.1 software.

REFERENCES

- [1] Patel, C. K.; Singh, S.; Saini, B.; Mukherjee, T. K. Macromolecular Crowding-Induced Unusual Liquid–Liquid Phase Separation of Human Serum Albumin via Soft Protein-Protein Interactions. *J. Phys. Chem. Lett.* **2022**, *13*, 3636–3644.
- [2] Mandeville, J. S.; Tajmir-Riahi, H. A. Complexes of Dendrimers with Bovine Serum Albumin. *Biomacromolecules* **2010**, *11*, 465–472.
- [3] Domínguez, M.; Cortés-Figueroa, J. E.; Meléndez, E. Biological Interaction of Molybdenocene Dichloride with Bovine Serum Albumin Using Fluorescence Spectroscopy. *Journal of Chemical Education* **2017**, *95*, 152–157
- [4] Mandeville, J. S.; Tajmir-Riahi, H. A. Complexes of Dendrimers with Bovine Serum Albumin. *Biomacromolecules* **2010**, *11*, 465–472.
- [5] Anderson, N. L.; Anderson, N. G. The Human Plasma Proteome: History, Character, and Diagnostic Prospects. *Molecular & cellular proteomics: MCP* **2002**, *1*, 845–867.
- [6] E.L. Gelamo, C.H.T.P. Silva, H. Imasato, M. Tabak, Interaction of bovine (BSA) and human (HSA) serum albumins with ionic surfactants: spectroscopy and modelling, *Biochimica et Biophysica Acta* **2002**, *1594* 84-99.
- [7] Reynolds, J. A., Herbert, S., Polet, H., & Steinhardt, J. The binding of divers detergent anions to bovine serum albumin. *Biochemistry* **1967**, *6*, 937-947.
- [8] Sklar, L. A., Hudson, B. S., & Simoni, R. D. Conjugated polyene fatty acids as fluorescent probes: binding to bovine serum albumin. *Biochemistry* **1977**, *16*, 5100-5108.
- [9] Steinhardt, J., Krijn, J., & Leidy, J. G. Differences between bovine and human serum albumins. Binding isotherms, optical rotatory dispersion,

- viscosity, hydrogen ion titration, and fluorescence effects. *Biochemistry* **1971**, *10*, 4005-4015.
- [10] Yamasaki, M., Yamashita, T., Yano, H., Tatsumi, K., & Aoki, K. Differential scanning calorimetric studies on bovine serum albumin IV. Effect of anionic surfactants with various lengths of hydrocarbon chain. *International journal of biological macromolecules* **1996**, *19*, 241-246.
- [11] Saini, B., & Mukherjee, T. K. Biomolecular condensates regulate enzymatic activity under a crowded milieu: synchronization of liquid—liquid phase separation and enzymatic transformation. *The Journal of Physical Chemistry B* **2023**, *127*, 180-193.
- [12] Smith, R. D., Engdahl, A. L., Dunbar Jr, J. B., & Carlson, H. A. Biophysical limits of protein–ligand binding. *Journal of chemical information and modeling*, **2012**, *52*, 2098-2106.
- [13] Choi, H. J., Lee, J. Y., & Kim, K. Glutathionylation on RNA-binding proteins: a regulator of liquid–liquid phase separation in the pathogenesis of amyotrophic lateral sclerosis. *Experimental & Molecular Medicine* **2023**, *55*, 735-744.
- [14] Patel, C. K.; Rani, C.; Kumar, R.; Mukherjee, T. K. Macromolecular Crowding Promotes Re-Entrant Liquid–Liquid Phase Separation of Human Serum Transferrin and Prevents Surface-Induced Fibrillation. *Biomacromolecules* **2023**, *24*, 3917–3928.
- [15] Patel, C. K.; Mallik, A.; Rath, D. K.; Kumar, R.; Mukherjee, T. K. Coalescence-Driven local crowding promotes Liquid-to-Solid-Like phase transition in a homogeneous and heterogeneous droplet assembly. *bioRxiv* **2024**, https://doi.org/10.1101/2024.10.08.617323.

- [16] Ray, S., Singh, N., Kumar, R., Patel, K., Pandey, S., Datta, D., ... & Maji, S. K. α-Synuclein aggregation nucleates through liquid–liquid phase separation. *Nature chemistry*, **2020**, *12*, 705-716.
- [17] Dogra, P., Joshi, A., Majumdar, A., & Mukhopadhyay, S. Intermolecular charge-transfer modulates liquid—liquid phase separation and liquid-to-solid maturation of an intrinsically disordered pH-responsive domain. *Journal of the American Chemical Society*, **2019**, *141*, 20380-20389.
- [18] Wegmann, S., Eftekharzadeh, B., Tepper, K., Zoltowska, K. M., Bennett, R. E., Dujardin, S., ... & Hyman, B. T. Tau protein liquid–liquid phase separation can initiate tau aggregation. *The EMBO journal*, **2018**, *37*, e98049.
- [19] Nilsson, S. Interactions between water-soluble cellulose derivatives and surfactants. 1. The HPMC/SDS/water system. *Macromolecules*, **1995**, 28, 7837-7844.
- [20] Shah, S. K., & Bhattarai, A. Interfacial and micellization behavior of cetyltrimethylammonium bromide (CTAB) in water and methanol-water mixture at 298.15 to 323.15 K. *Journal of Chemistry*, **2020**, 2020, 4653092.
- [21] Belarbi, H., & Bouanani, F. Interfacial and micellar synergistic interactions between a phosphonium surface active ionic liquid and TX-100 nonionic surfactant: Surface tension and 1H NMR investigations. *Journal of Molecular Liquids*, **2023**, *383*, 122060.
- [22] Rainsford, K. D. Ibuprofen: pharmacology, efficacy and safety. *Inflammopharmacology*, **2009**, *17*, 275-342.
- [23] Rettie, A. E., & Tai, G. The pharmocogenomics of warfarin. *Molecular interventions*, **2006**, *6*, 223.

- [24] Charbonneau, D., Beauregard, M., & Tajmir-Riahi, H. A. Structural analysis of human serum albumin complexes with cationic lipids. *The Journal of physical chemistry B*, **2009**, *113*, 1777-1784.
- [25] Mouritsen, O. G., & Zuckermann, M. J. What's so special about cholesterol? *Lipids*, **2004**, *39*, 1101-1113.
- [26] Regelin, A. E., Fankhaenel, S., Gürtesch, L., Prinz, C., von Kiedrowski, G., & Massing, U. Biophysical and lipofection studies of DOTAP analogs. *Biochimica et Biophysica Acta (BBA)-Biomembranes*, **2000**, *1464*(1), 151-164.